Targeting Ras-Driven Cancer Cell Survival and Invasion through Selective Inhibition of DOCK1

田尻, 裕匡

https://doi.org/10.15017/1866274

出版情報：Kyushu University, 2017, 博士（医学）, 課程博士
バージョン：

Article

Cell Reports

Targeting Ras-Driven Cancer Cell Survival and Invasion through Selective Inhibition of DOCK1

Graphical Abstract

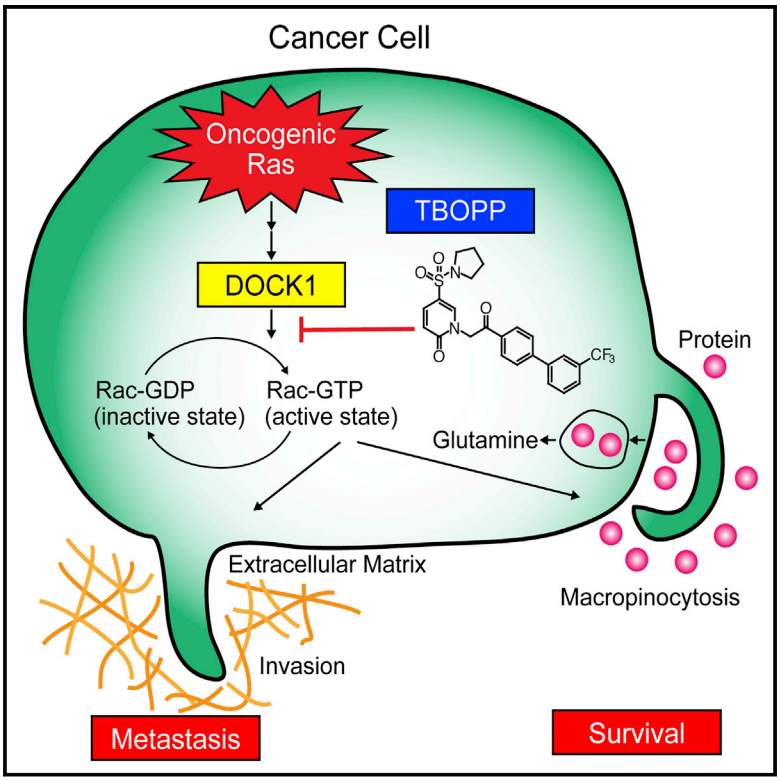

Highlights

- DOCK1 is a Rac activator critical for oncogenic Ras-induced cellular invasion
- DOCK1 controls macropinocytosis-dependent nutrient uptake in Ras-transformed cells
- TBOPP has been developed as a DOCK1-selective inhibitor
- TBOPP dampens DOCK1-mediated cellular functions in vitro and in vivo

Authors

Hirotada Tajiri, Takehito Uruno, Takahiro Shirai, ..., Shigeyuki Yokoyama, Motomu Kanai, Yoshinori Fukui

Correspondence

fukui@bioreg.kyushu-u.ac.jp

In Brief

Tajiri et al. find that the Rac-specific guanine nucleotide exchange factor DOCK1 is required for oncogenic Ras-driven nutrient uptake and cellular invasion. Through chemical library screening, they identify TBOPP as a DOCK1-selective inhibitor that suppresses growth and metastasis of Ras-transformed cancer cells in vivo.

Tajiri et al., 2017, Cell Reports *19*, 969–980
May 2, 2017
http://dx.doi.org/10.1016/j.celrep.2017.04.016

Cell Reports
Article

Targeting Ras-Driven Cancer Cell Survival and Invasion through Selective Inhibition of DOCK1

Hirotada Tajiri,[1,2,11] Takehito Uruno,[1,3,11] Takahiro Shirai,[4] Daisuke Takaya,[5] Shigeki Matsunaga,[6] Daiki Setoyama,[7] Mayuki Watanabe,[1,3,12] Mutsuko Kukimoto-Niino,[5] Kounosuke Oisaki,[4] Miho Ushijima,[1] Fumiyuki Sanematsu,[1,3] Teruki Honma,[5] Takaho Terada,[8] Eiji Oki,[2] Senji Shirasawa,[9] Yoshihiko Maehara,[2] Dongchon Kang,[7] Jean-François Côté,[10] Shigeyuki Yokoyama,[8] Motomu Kanai,[4] and Yoshinori Fukui[1,3,13,*]

[1]Division of Immunogenetics, Department of Immunobiology and Neuroscience, Medical Institute of Bioregulation, Kyushu University, Fukuoka 812-8582, Japan
[2]Department of Surgery and Science, Graduate School of Medical Sciences, Kyushu University, Fukuoka 812-8582, Japan
[3]Research Center for Advanced Immunology, Kyushu University, Fukuoka 812-8582, Japan
[4]Graduate School of Pharmaceutical Sciences, The University of Tokyo, Tokyo 113-0033, Japan
[5]RIKEN Center for Life Science Technologies, Yokohama 230-0045, Japan
[6]Faculty of Pharmaceutical Sciences, Hokkaido University, Sapporo 060-0812, Japan
[7]Department of Clinical Chemistry and Laboratory Medicine, Graduate School of Medical Sciences, Kyushu University, Fukuoka 812-8582, Japan
[8]RIKEN Structural Biology Laboratory, Yokohama 230-0045, Japan
[9]Department of Cell Biology, Faculty of Medicine, Fukuoka University, Fukuoka 814-0180, Japan
[10]Institut de Recherches Cliniques de Montréal (Université de Montréal), Montréal, QC H2W 1R7, Canada
[11]These authors contributed equally
[12]Present address: Department of Physiology and Pharmacology, Cumming School of Medicine, University of Calgary, Calgary, AB T2N 4N1, Canada
[13]Lead Contact
*Correspondence: fukui@bioreg.kyushu-u.ac.jp
http://dx.doi.org/10.1016/j.celrep.2017.04.016

SUMMARY

Oncogenic Ras plays a key role in cancer initiation but also contributes to malignant phenotypes by stimulating nutrient uptake and promoting invasive migration. Because these latter cellular responses require Rac-mediated remodeling of the actin cytoskeleton, we hypothesized that molecules involved in Rac activation may be valuable targets for cancer therapy. We report that genetic inactivation of the Rac-specific guanine nucleotide exchange factor DOCK1 ablates both macropinocytosis-dependent nutrient uptake and cellular invasion in Ras-transformed cells. By screening chemical libraries, we have identified 1-(2-(3′-(trifluoromethyl)-[1,1′-biphenyl]-4-yl)-2-oxoethyl)-5-pyrrolidinylsulfonyl-2(1*H*)-pyridone (TBOPP) as a selective inhibitor of DOCK1. TBOPP dampened DOCK1-mediated invasion, macropinocytosis, and survival under the condition of glutamine deprivation without impairing the biological functions of the closely related DOCK2 and DOCK5 proteins. Furthermore, TBOPP treatment suppressed cancer metastasis and growth in vivo in mice. Our results demonstrate that selective pharmacological inhibition of DOCK1 could be a therapeutic approach to target cancer cell survival and invasion.

INTRODUCTION

The small guanosine triphosphatases (GTPases) function as molecular switches by cycling between guanosine diphosphate (GDP)-bound inactive and guanosine triphosphate (GTP)-bound active states (Colicelli, 2004; Sahai and Marshall, 2002; Van Aelst and D'Souza-Schorey, 1997). Stimulus-induced activation of small GTPases is mediated by guanine nucleotide exchange factors (GEFs), and once activated, they bind to a variety of effector molecules to regulate various cellular functions, including proliferation, differentiation, survival, migration, and transformation (Colicelli, 2004; Sahai and Marshall, 2002; Van Aelst and D'Souza-Schorey, 1997). The small GTPases comprise more than 150 members in humans (Colicelli, 2004), and they are classified into five subgroups: Ras, Ran, Rho, Rab, and Arf families. Among them, *RAS* is the gene most frequently mutated in human tumors. Accumulating evidence indicates that mutations activating RAS family members, K-RAS, H-RAS, and N-RAS, are found in 20%–30% of human tumors (Cox et al., 2014; Prior et al., 2012; Spiegel et al., 2014), thereby placing these mutations as major drivers of cancers. However, despite intense efforts for more than three decades (Cox et al., 2014; Spiegel et al., 2014), attempts to inhibit oncogenic Ras have not been successful.

Oncogenic Ras plays a key role in cancer initiation, but also contributes to malignant phenotypes in several ways. For example, oncogenic Ras stimulates uptake of extracellular proteins by means of macropinocytosis to supply amino acids including glutamine (Commisso et al., 2013). A hallmark of Ras-transformed cells is their use of glutamine as the main

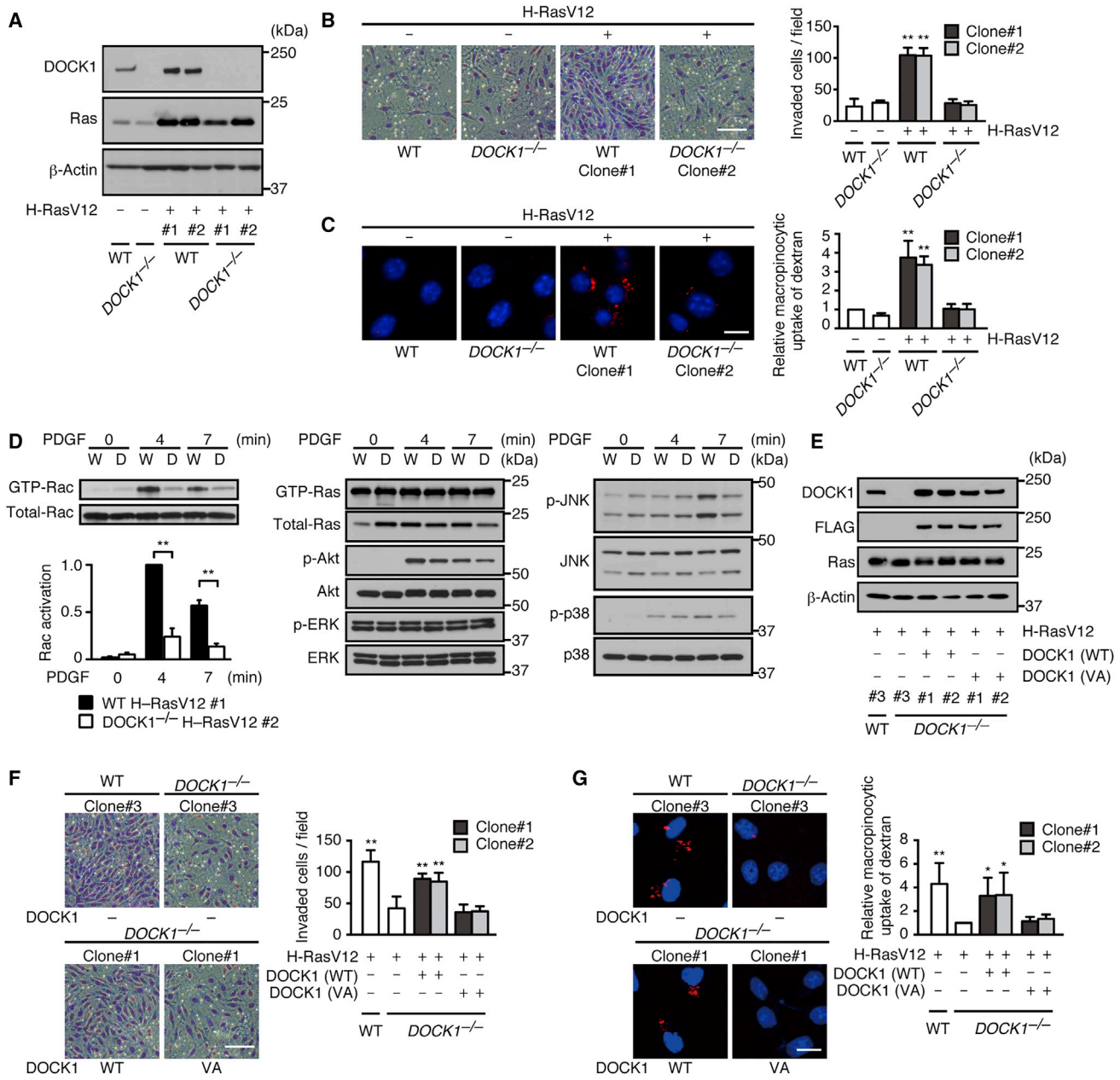

Figure 1. DOCK1 Is Required for Oncogenic Ras-Induced Cellular Functions in MEFs

(A) Western blot analysis for the expression of DOCK1 and Ras in WT and *Dock1*$^{-/-}$ MEFs with or without exogenous H-RasV12 expression. The numerals (#) indicate the clone number.

(B) Comparison of invasive activity among WT and *Dock1*$^{-/-}$ MEFs with or without H-RasV12 expression. In each experiment, the number of invaded cells per field was determined by counting cells in four distinct fields. Scale bar, 100 μm. Data are expressed as mean ± SD of five independent experiments. **$p < 0.01$ compared with WT samples without H-RasV12 expression (ANOVA followed by Dunnett's post hoc test).

(C) Comparison of macropinocytic uptake of dextran (red) among WT and *Dock1*$^{-/-}$ MEFs with or without H-RasV12 expression. DAPI (blue) was used to stain nuclei. Scale bar, 20 μm. Data (mean ± SD, n = 5) are expressed as the relative index after normalization of the WT level without H-RasV12 expression to an arbitrary value of 1. **$p < 0.01$ compared with WT samples without H-RasV12 expression (ANOVA followed by Dunnett's post hoc test).

(D) Activation of Rac, Ras, and other signaling molecules in response to PDGF stimulation in H-RasV12-expressing WT (W) and *Dock1*$^{-/-}$ (D) MEFs. Data are representative of three or four independent experiments. p, phosphorylated molecule. For Rac activation, results were quantified by densitometry and are expressed as the ratio of the GTP-bound form to the total protein after normalization (4 min value of WT MEFs to an arbitrary value of 1). Data are expressed as mean ± SD (n = 4). **$p < 0.01$ (two-tailed unpaired Student's t test).

(E) Western blot analysis for the expression of endogenous and exogenous DOCK1 (FLAG-tagged WT or V1534A mutant) in H-RasV12-expressing WT and *Dock1*$^{-/-}$ MEFs.

(legend continued on next page)

carbon source for tricarboxylic acid (TCA) cycle (White, 2013; Ying et al., 2012). To ensure glutamine uptake, these cancer cells exploit macropinocytosis induced by oncogenic Ras to sustain their growth and survival (Commisso et al., 2013). Macropinocytosis is a unique mode of endocytosis, which occurs via induction of membrane ruffles, especially circular ruffles (Buccione et al., 2004; Hoon et al., 2012). In addition, circular ruffles are involved in three-dimensional cell migration (Suetsugu et al., 2003), and their relationship to the invasive leading edge in cancer cells has been highlighted (Buccione et al., 2004; Hoon et al., 2012). It is known that matrix-degrading matrix metalloproteinase-2 (MMP-2) localizes at the tips of circular ruffles and promotes cell invasion into the extracellular matrix (Suetsugu et al., 2003). Thus, oncogenic Ras controls survival and invasion of cancer cells through remodeling of the actin cytoskeleton, which is dependent on the activity of the Rho family GTPase Rac (Lanzetti et al., 2004; Suetsugu et al., 2003; Zwartkruis and Burgering, 2013). Accordingly, genetic or functional ablation of Rac1 suppresses oncogenic Ras-induced transformation and cancer development (Heid et al., 2011; Kissil et al., 2007; Qiu et al., 1995). However, the ubiquitous expression of Rac isoforms and their similarity to Ras preclude using Rac proteins as molecular targets for cancer therapy. One attractive approach is to identify and chemically target the molecules responsible for Rac activation downstream of oncogenic Ras.

How oncogenic Ras promotes Rac activation is poorly defined, but this process likely involves direct or indirect activation of Rac GEFs. There are two distinct families of Rac GEFs: Dbl-homology (DH) domain-containing proteins and DOCK proteins (Laurin and Côté, 2014; Schmidt and Hall, 2002). Until recently, DH domain-containing proteins have been considered the universal GEFs in eukaryotes. However, accumulating evidence indicates that the DOCK proteins act as major Rac GEFs in various biological settings. For example, DOCK2, which is predominantly expressed in hematopoietic cells, plays key roles in migration and activation of leukocytes (Fukui et al., 2001; Gotoh et al., 2008, 2010; Kunisaki et al., 2006; Nishikimi et al., 2009; Sanui et al., 2003). However, DOCK1 (also known as DOCK180) and DOCK5 are widely expressed in various tissues and regulate phagocytosis, myoblast fusion, and cell migration (Grimsley et al., 2004; Gumienny et al., 2001; Laurin et al., 2008; Li et al., 2008; Sanematsu et al., 2010). Although these molecules do not contain DH domain, they mediate the GTP-GDP exchange reaction for Rac through the DOCK homology region 2 (DHR-2, also known as Docker or CZH2) domain (Kulkarni et al., 2011; Laurin and Côté, 2014).

We postulate that the inhibition of the relevant Rac GEFs may have a therapeutic benefit in cancers harboring Ras mutations. DOCK1 is a strong candidate, because its expression is associated with malignant phenotypes in many cancers (Jarzynka et al., 2007; Laurin et al., 2013; Wang et al., 2010; Zhao et al., 2011). Several lines of evidence indicate that DOCK1 regulates invasive migration and metastasis of cancer cells by acting downstream of oncogenic receptor tyrosine kinases (RTKs) (Feng et al., 2011, 2012; Laurin et al., 2013). In addition, it has been shown that DOCK1 is a Rac GEF essential for RTK-induced circular ruffle formation in mouse embryonic fibroblasts (MEFs), although the formation of peripheral ruffles is coordinated by both DOCK1 and DOCK5 (Sanematsu et al., 2013). We found that genetic inactivation of DOCK1 in Ras-transformed cells ablates macropinocytosis-dependent nutrient uptake and cellular invasion. To test the notion that DOCK1 may be a target for cancer therapy, we screened chemical libraries and identified 1-(2-(3′-(trifluoromethyl)-[1,1′-biphenyl]-4-yl)-2-oxoethyl)-5-pyrrolidinylsulfonyl-2(1*H*)-pyridone (designated TBOPP) as a DOCK1-selective inhibitor. By analyzing its effect in cells and mice, we show here that the pharmacological inhibition of DOCK1 could be a therapeutic approach to target cancer cell survival and invasion.

RESULTS

Role of DOCK1 in Ras-Induced Cellular Functions in Transformed MEFs

To examine the role of DOCK1 in Ras-induced cellular functions, we prepared Simian virus 40 (SV40)-transformed wild-type (WT) and DOCK1-deficient (*Dock1*$^{-/-}$) MEFs (Figure 1A). When the constitutively active H-Ras that has valine instead of glycine at position 12 (H-RasV12) was expressed in WT MEFs, cell invasion was increased approximately 4.5-fold in two independent clones (Figure 1B). Similarly, the expression of H-RasV12 in WT MEFs augmented macropinocytosis more than 3.3-fold, compared with that of non-transfected WT MEFs (Figure 1C). In contrast, neither invasion nor macropinocytosis increased in MEFs by overexpressing WT Ras (Figure S1). Although DOCK1 deficiency in H-RasV12-expressing MEFs significantly reduced Rac1 activation in response to platelet-derived growth factor (PDGF) (Figure 1D), activations of other signaling cascades, including Ras GTP loading and AKT/ERK/JNK/p38 phosphorylation, were not significantly changed between WT and *Dock1*$^{-/-}$ MEFs (Figure 1D). However, the oncogenic Ras-induced invasion and macropinocytosis were markedly suppressed in *Dock1*$^{-/-}$ MEFs (Figures 1B and 1C). When WT DOCK1 was expressed in *Dock1*$^{-/-}$ MEFs, both Ras-induced invasion and macropinocytosis were restored to the levels of WT MEFs (Figures 1E–1G). In contrast, the defects in invasion and macropinocytosis were not rescued by expressing the GEF-dead mutant V1534A encoding alanine instead of valine at position 1,534 (Figures 1E–1G) (Kulkarni et al., 2011). These results indicate that DOCK1 regulates key Ras-induced cellular functions by acting as a Rac GEF.

(F) Rescue of H-RasV12-induced invasive activity of *Dock1*$^{-/-}$ MEFs by expression of WT DOCK1, but not V1534A mutant (VA). Scale bar, 100 μm. Data are expressed as mean ± SD of five independent experiments. **p < 0.01 compared with *Dock1*$^{-/-}$ MEFs without DOCK1 add back (ANOVA followed by Dunnett's post hoc test).

(G) Rescue of H-RasV12-induced macropinocytosis in *Dock1*$^{-/-}$ MEFs by expression of WT DOCK1, but not V1534A mutant (VA). Scale bar, 20 μm. Data (mean ± SD, n = 5) are expressed as the relative index after normalization of the level of *Dock1*$^{-/-}$ MEFs without DOCK1 add back to an arbitrary value of 1. *p < 0.05, **p < 0.01 compared with *Dock1*$^{-/-}$ MEFs without DOCK1 add back (ANOVA followed by Dunnett's post hoc test).

See also Figure S1.

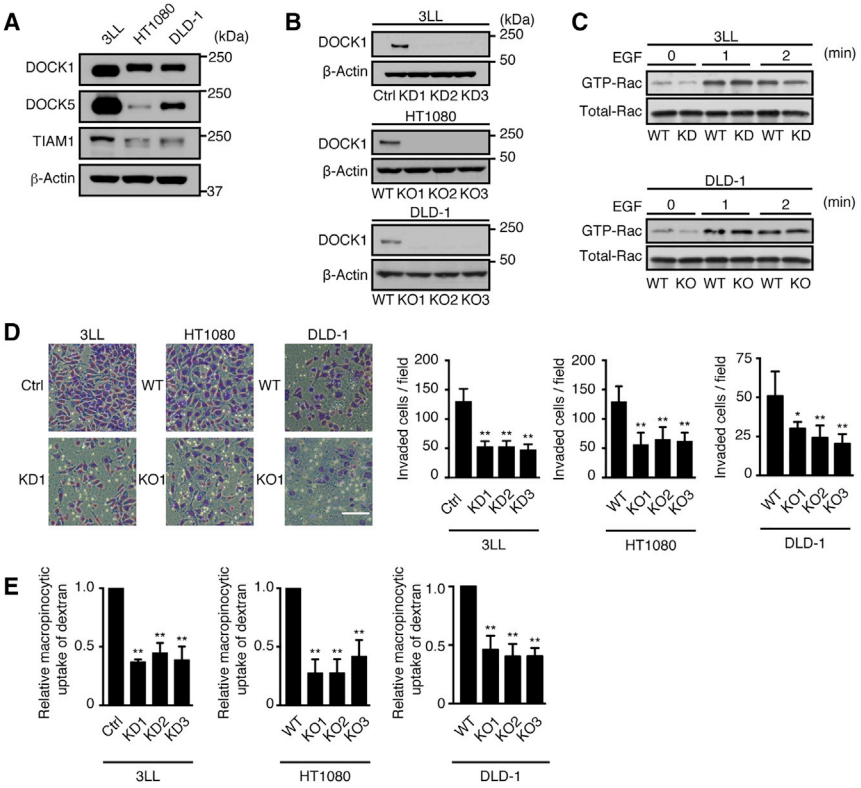

Figure 2. DOCK1 Deficiency Suppresses Invasion and Macropinocytosis of Cancer Cells

(A) Western blot analysis for the expression of DOCK1, DOCK5 and TIAM1, in 3LL, HT1080, and DLD-1 cancer cell lines. As a control, β-actin expression is shown.

(B) Western blot analysis for the expression of DOCK1 in 3LL-KD, HT1080-KO, DLD-1-KO, and their parent or control cells. As a control of 3LL-KD (Ctrl), 3LL cells transfected with the shRNA-targeting irrelevant *lacZ* sequence were used.

(C) Comparison of EGF-induced Rac activation in 3LL and DLD-1 cells with (WT) or without (KD or KO) DOCK1 expression.

(D) Comparison of invasive activity among 3LL-KD, HT1080-KO, DLD-1-KO, and their parent or Ctrl cells. In each experiment, the number of invaded cells per field was determined by counting cells in four distinct fields. Scale bar, 100 μm. Data are expressed as mean ± SD of five independent experiments. *$p < 0.05$, **$p < 0.01$ compared with Ctrl or WT samples (ANOVA followed by Dunnett's post hoc test).

(E) Comparison of macropinocytic uptake of dextran among 3LL-KD, HT1080-KO, DLD-1-KO, and their parent or Ctrl cells. Data (mean ± SD, n = 5) are expressed as the relative index after normalization of the Ctrl or WT level to an arbitrary value of 1. **$p < 0.01$ compared with Ctrl or WT samples (ANOVA followed by Dunnett's post hoc test).

See also Figures S2 and S3.

Effect of DOCK1 Deficiency on Invasion and Survival of Cancer Cells

To examine whether the effect of DOCK1 deficiency could be applied to cancer cells, we used a mouse Lewis lung carcinoma cell line 3LL, a human sarcoma cell line HT1080, and a human colon cancer cell line DLD-1, each of which harbors the oncogenic mutation at the K-Ras (G12C), N-RAS (Q61K), and K-RAS (G13D) locus, respectively (Kawazu et al., 2013; Shirasawa et al., 1993). All these cancer cells express not only DOCK1 but also other Rac GEFs, such as DOCK5 and TIAM1, the latter of which is known to act downstream of oncogenic Ras (Figure 2A) (Malliri et al., 2002). When DOCK1 expression was knocked down in 3LL cells (designated 3LL-KD) by short hairpin RNA (shRNA) (Figure 2B), neither the basal nor the epidermal growth factor (EGF)-induced Rac activation was significantly affected in pull-down assays (Figure 2C), probably because of functional compensation of the other Rac GEFs. In addition, in vitro proliferation was only modestly changed between 3LL and 3LL-KD cells under normal culture condition (Figure S2). Nonetheless, DOCK1 knockdown in 3LL cells markedly suppressed invasion to the extracellular matrix and macropinocytosis of dextran (Figures 2D and 2E). Similar results were obtained by genetically deleting *DOCK1* in HT1080 (designated HT1080-KO) and DLD-1 (designated DLD-1-KO) cells by using the CRISPR/Cas9 nuclease system (Figures 2B–2E). In contrast, ablating TIAM1 expression in DLD-1 cells had no impact on invasion or macropinocytosis (Figures S3A–S3C). It is clear that oncogenic Ras stimulates invasion and macropinocytosis, because these cellular functions were suppressed in DLD-1 cells when mutant, but not WT, *K-RAS* allele was disrupted by homologous recombination (DLD-1 HR-M) (Figures S3D and S3E) (Shirasawa et al., 1993). Collectively, these results indicate that DOCK1 deficiency alone is effective for suppressing invasion of and macropinocytosis in Ras-transformed cancer cells.

It is well known that Ras-transformed cells have elevated dependence on glutamine for their growth and survival (Gaglio et al., 2009; Wu et al., 1978). Because recent evidence indicates that macropinocytosis of extracellular proteins is a major route to supply glutamine in cancer cells (Commisso et al., 2013), we next compared the viability of cancer cells under the condition of glutamine deprivation. Although 3LL cells exhibited impaired cell viability when cultured in media containing a subphysiological concentration of glutamine (0.22 mM), addition of dialyzed fetal calf serum (dFCS) to the culture restored cell viability (Figure 3A), because it could serve as a source of glutamine after cellular uptake via macropinocytosis. However, such an effect of dFCS addition was not seen for 3LL-KD cells (Figure 3A). Similar results were obtained when HT1080-KO, DLD-1-KO, and *Dock1*$^{-/-}$ H-RasV12-expressing MEFs were analyzed (Figure 3A). More importantly, treatment with bis-2-(5-phenylacetamido-1,3,4-thiadiazol-2-yl)ethyl sulfide (BPTES), an inhibitor of glutaminase (Robinson et al., 2007), markedly increased the glutamine content in 3LL, but not 3LL-KD, cells when cultured in the presence of dFCS (Figure 3B). Thus, DOCK1 is required for Ras-transformed cancer cells to sustain growth and survival under the condition of glutamine deprivation.

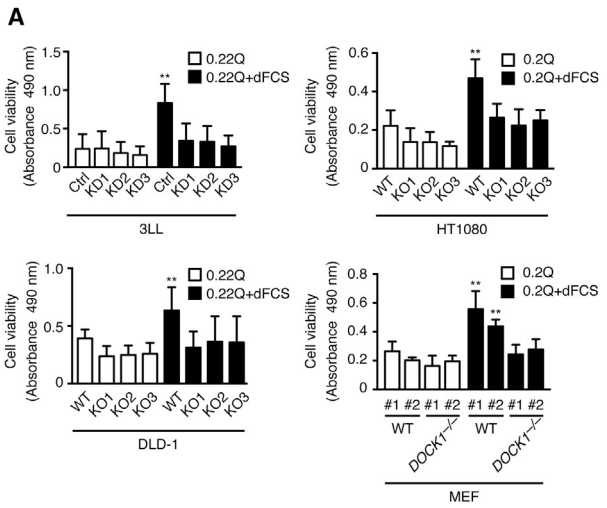

Figure 3. DOCK1 Deficiency Suppresses Growth and Survival of Cancer Cells under the Condition of Glutamine Deprivation

(A) Comparison of cell viability among 3LL-KD, HT1080-KO, DLD-1-KO, *Dock1*$^{-/-}$ H-RasV12-expressing-MEFs, and their parent or Ctrl cells under the condition of glutamine deprivation (0.22 mM; designated 0.22Q) with or without dFCS addition. Data are expressed as mean ± SD of 5 (3LL and HT-1080), 6 (H-RasV12-expressing-MEFs), or 11 (DLD-1) independent experiments. **p < 0.01 compared with Ctrl or WT samples without dFCS addition (ANOVA followed by Dunnett's post hoc test).

(B) Comparison of cellular content of glutamine in 3LL-KD and Ctrl cells under the condition of glutamine deprivation (0.22Q) with or without dFCS addition. In some experiments, cells were treated with BPTES. Data (mean ± SD, n = 5) are expressed as the relative index after normalization of the Ctrl level without dFCS addition to an arbitrary value of 1. *p < 0.05, **p < 0.01 compared with Ctrl samples without dFCS addition (ANOVA followed by Dunnett's post hoc test).

Screening and Identification of DOCK1-Selective Inhibitors

Having found that DOCK1 deficiency effectively suppresses oncogenic Ras-induced malignant phenotypes in cancer cells, we aimed to develop small-molecule inhibitors of DOCK1 using a computational docking strategy (Figure S4). Because the structural information of DOCK1 DHR-2 domain was unavailable, we first screened in silico 202,789 compounds for the Rac1 binding site of DOCK2 to select putative DOCK inhibitors. To complement this approach, we also performed similarity searches using 4-[3′-(2′-chlorophenyl)-2′-propen-1′-ylidene]-1-phenyl-3,5-pyrazolidinedione (CPYPP) (Nishikimi et al., 2012), which we previously identified as a compound that equally inhibits the Rac GEF activity of DOCK1, DOCK2, and DOCK5. After filtering and clustering (see Supplemental Experimental Procedures), we selected 673 compounds (91 compounds from the similarity search and 584 compounds from the docking calculation; 2 compounds were selected by both approaches) as new candidates of DOCK inhibitors. Of these, 567 compounds were publicly available. By experimentally testing their inhibitory effects for the Rac GEF activity of DOCK1, DOCK2, and DOCK5, we found that 1-(2-(1-(4-fluorobenzyl)-2,5-dimethyl-1*H*-pyrrol-3-yl)-2-oxoethyl)-5-(pyrrolidin-1-ylsulfonyl)pyridin-2(1*H*)-one (FDOPP, compound **1**) preferentially inhibited DOCK1-mediated Rac activation, without affecting Rac GEF activity of Trio and Tiam1 (Figures 4A and 4B).

This finding led us to examine the structure of FDOPP required for its inhibitory activity. For this purpose, we synthesized FDOPP analogs and compared their effects on the Rac GEF activity of DOCK proteins. Compound **2** lacking the sulfonamide fragment resulted in complete loss of inhibitory activity (Figure 5), indicating that the sulfonamide fragment is essential. Among the sulfonamide units screened, sulfonamide derived from pyrrolidine showed a good result (Figure 5). When the N-benzyl pyrrole unit was replaced with N-methyl pyrrole (compound **4**) or with a simple phenyl ring (compound **5**), inhibitory activity was abolished (Figure 5). However, compound **6** bearing a biphenyl unit kept inhibitory activity and showed improved DOCK1 selectivity in comparison with FDOPP (Figure 5). Based on these findings, we synthesized a variety of substituted biphenyl derivatives via cross-coupling reactions and compared their inhibitory activities and DOCK1 selectivity. Among 16 compounds tested (compounds **7**–**22**) (Figure 5), TBOPP (compound **16**) bearing CF_3 group at *m*-position (meta-CF_3) substituent showed the best result in terms of potency and DOCK1 selectivity (Figures 4A, 4B, 5, and S5). Surface plasmon resonance (SPR)-based binding assays revealed that TBOPP, but not compound **5**, bound to DOCK1 DHR-2 domain with high affinity (K_d = 7.1 μM) (Figures 4C and 4D). However, its binding affinity was significantly lower for DOCK2 DHR-2 domain (K_d = 56.8 μM) or Tiam1 DH-pleckstrin homology (PH) domain (K_d = 233.3 μM). Consistent with this finding, TBOPP treatment abrogated the association between DOCK1 and Rac1, without affecting Tiam1-Rac1 interaction (Figure 4E). As seen in 3LL-KD and DLD-1-KO cells (Figure 2C), treatment of 3LL or DLD-1 cells with TBOPP did not significantly affect EGF-induced Rac activation in pull-down assays (Figure S6). However, when WT MEFs expressing H-RasV12 were treated with TBOPP, PDGF-induced Rac activation was reduced to the level of *Dock1*$^{-/-}$ MEFs (Figure S6), indicating that TBOPP is a cell-active compound. Therefore, TBOPP was selected and synthesized in gram scale for further evaluation (Figure 4F).

Blockade of Cancer Cell Invasion and Survival In Vitro by TBOPP

We first examined the effect of TBOPP on cancer cell invasion in vitro. When 3LL, HT1080, and DLD-1 cells were treated with TBOPP at 12.5 μM for 22–28 hr, invasion to the extracellular matrix was markedly reduced (Figure 6A), despite cell viability being unaffected (Figure 6B). However, no such inhibitory effect was seen with compound **5** (Figure 6A). The same concentration of TBOPP did not affect CCL21-induced lymphocyte migration (Figure 6C), which is known to rely exclusively on DOCK2 activity

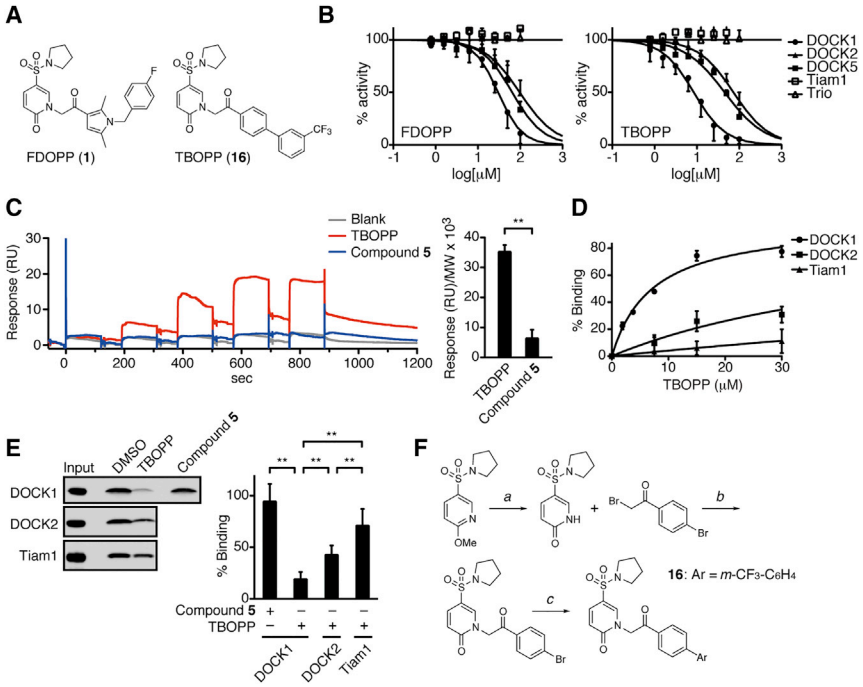

Figure 4. Structure, Function, and Synthesis of FDOPP and TBOPP

(A) Structure of FDOPP (compound **1**) and TBOPP (compound **16**).

(B) Comparison of inhibitory activities of FDOPP and TBOPP for various Rac GEFs. Dose-response curves of FDOPP and TBOPP are shown for their effects on Rac activation by DHR-2 domain (DOCK1, DOCK2, and DOCK5) and DH-PH domain (Trio and Tiam1). Data are expressed as mean ± SD of three or four independent experiments after normalization of the value of the Ctrl sample treated with vehicle alone as 100%.

(C) SPR-based binding assay showing that TBOPP, but not compound **5**, binds to DOCK1 DHR-2 domain in a reversible manner. TBOPP or compound **5** was tested at 1.875, 3.75, 7.5, 15, and 30 μM from the left to the right. The plot indicates the response level at 15 μM of each compound after normalization by dividing the measured RUs by the molecular weight (MW). Data are expressed as mean ± SD of three independent experiments. **p < 0.01 (two-tailed unpaired Student's t test).

(D) Titration curve for TBOPP binding to DOCK1 DHR-2, DOCK2 DHR-2, and Tiam DH-PH proteins. For comparison, the RUs obtained from three or four independent experiments were converted to percentage of binding relative to the maximal binding level of each protein. Based on this curve, K_d of TBOPP binding for each protein was determined.

(E) Effect of TBOPP on the association between Rac1 and DOCK1 DHR-2, DOCK2 DHR-2, or Tiam DH-PH. Blots show His-SUMO-tagged proteins before (input) and after pull-down assays in the presence of TBOPP, compound **5**, or vehicle alone (DMSO). Data are expressed as mean ± SD of five or seven independent experiments after normalization of the value of Ctrl sample treated with vehicle alone as 100%. **p < 0.01 (two-tailed unpaired Student's t test).

(F) Synthesis of TBOPP (compound **16**). Reagents and conditions: a, KI, $(CH_3)_3SiCl$, CH_3CN, reflux; b, NaH, tetrahydrofuran (THF), 60°C, 9% (2 steps); c, $Pd(OAc)_2$ (10 mol %), 1,1′-bis(diphenylphosphino)ferrocene (10 mol %), $ArB(OH)_2$, K_3PO_4, toluene/H_2O, 100°C, 92% for TBOPP.

See also Figures S4–S7.

(Fukui et al., 2001). We also found that PDGF-induced peripheral ruffles in MEFs, which are regulated by the redundant activity of DOCK1 and DOCK5 (Sanematsu et al., 2013), was comparable between TBOPP-treated and non-treated samples (Figure 6D). In contrast, the formation of circular ruffles, which requires DOCK1, but not DOCK5, activity (Sanematsu et al., 2013), was markedly impaired by TBOPP treatment (Figure 6D). Consistent with this defect, macropinocytosis of dextran was reduced in TBOPP-treated cancer cell lines (Figure 6E), resulting in failure to survive under the condition of glutamine deprivation even when dFCS was added to the culture (Figure 6F). Collectively, these results indicate that treatment with TBOPP inhibits DOCK1-dependent invasion of and macropinocytosis in cancer cells, without affecting cellular functions of the closely related Rac GEFs DOCK2 and DOCK5.

Treatment with TBOPP Suppresses Cancer Metastasis and Growth In Vivo

To examine whether the usefulness of TBOPP could be extended to in vivo situations, we examined ex-3LL, a 3LL-derivative cell line with high metastatic property. Two weeks after intravenous injection of ex-3LL cells into C57BL/6 mice (Figure 7A), the metastatic foci were readily detected in the lung and the total lung weight increased (Figures 7B and 7C). However, the lung metastasis was significantly suppressed by treating C57BL/6 mice with 0.67 mg of TBOPP four times (Figures 7B and 7C). During TBOPP treatment, the number of lymphocytes in the spleen was not changed, demonstrating that this drug does not inhibit DOCK2 in vivo (Figure 7D). The body weight was also unchanged between TBOPP-treated and non-treated mice (Figure 7E), strongly suggesting that this compound is well tolerated in vivo. In addition, we found that continuous intravenous administration of TBOPP using a programmable infusion pump markedly suppressed in vivo growth of 3LL and DLD-1 cells in BALB/c nude mice (Figure 7F), without affecting B cell numbers in the spleen (Figure 7G). Thus, TBOPP can effectively suppress metastasis and growth of cancer cells in vivo, even though they have oncogenic Ras mutations.

DISCUSSION

Oncogenic Ras contributes to malignant phenotypes in cancer cells by stimulating nutrient uptake and promoting invasive migration. Because these cellular responses depend on Rac-mediated remodeling of the actin cytoskeleton (Lanzetti et al., 2004; Suetsugu et al., 2003; Zwartkruis and Burgering, 2013), we hypothesized that molecules involved in Rac activation would be candidate targets for cancer therapy. In this study, we have shown that genetic inactivation of DOCK1 in Ras-transformed cells ablates macropinocytosis-dependent uptake of nutrients

Effect of substitution on X

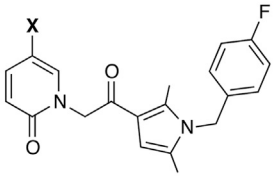

	X	IC_{50}, μM (Selectivity) D1	D2	D5
1 (FDOPP)	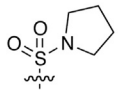	30.0	97.2. (3.2)	64.5 (2.2)
2	H	>300	>300	>300
3	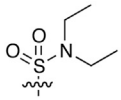	45.4	167.3 (3.7)	78.3 (1.7)

Effect of substitution on Y

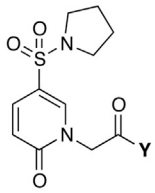

	Y	IC_{50}, μM (Selectivity) D1	D2	D5
4	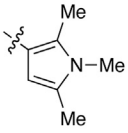	>300	>300	>300
5		>300	>300	>300
6	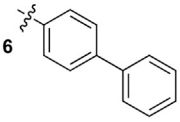	27.5	155.9 (5.7)	199.7 (7.3)

	Y	IC_{50}, μM (Selectivity) D1	D2	D5
7	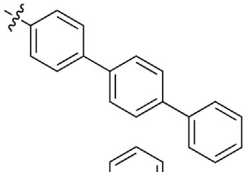	12.5	50.3 (4.0)	23.4 (1.9)
8	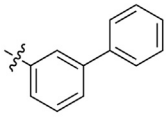	13.9	38.7 (2.8)	27.0 (1.9)

Effect of substitution on Z

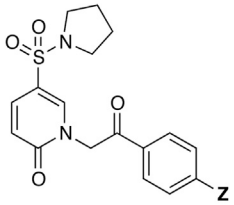

	Z	IC_{50}, μM (Selectivity) D1	D2	D5
9	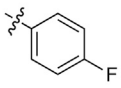	35.4	93.9 (2.7)	49.1 (1.4)
10	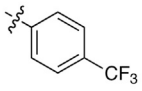	40.5	253.2 (6.3)	94.8 (2.3)
11	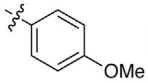	28.8	307.2 (10.7)	43.1 (1.5)
12	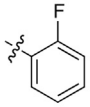	36.6	117.3 (3.2)	95.0 (2.6)
13	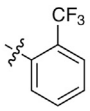	15.8	54.3 (3.4)	58.2 (3.7)

	Z	IC_{50}, μM (Selectivity) D1	D2	D5
14	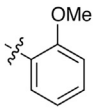	24.3	161.7 (6.7)	95.1 (3.9)
15	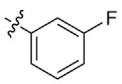	30.7	118.3 (3.9)	93.2 (3.0)
16 (TBOPP)	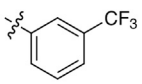	8.4	73.2 (8.7)	45.3 (5.4)
17	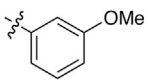	46.0	>300	70.1 (1.5)
18	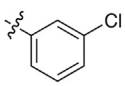	28.3	82.9 (2.9)	42.5 (1.5)

	Z	IC_{50}, μM (Selectivity) D1	D2	D5
19	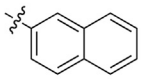	6.2	27.3 (4.4)	17.3 (2.8)
20	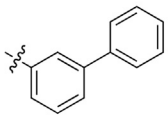	10.7	54.4 (5.1)	18.6 (1.7)
21	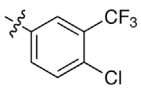	21.9	134.8 (6.2)	37.2 (1.7)
22	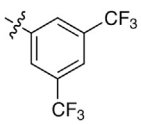	16.0	39.6 (2.5)	32.5 (2.0)

(legend on next page)

and impairs their growth and survival under the condition of glutamine deprivation. Similar inhibitory effects were observed when cellular invasion was compared. It is clear that DOCK1 regulates these cellular functions via Rac activation, because the expression of WT DOCK1, but not the GEF-dead DOCK1 mutant, in *Dock1*$^{-/-}$ MEFs rescued the defects in macropinocytosis and invasion. Thus, DOCK1 could be a molecular target for controlling Ras-induced malignant phenotypes, at least in certain cancer cells. It is unclear why DOCK1 plays a major role in macropinocytosis and invasion among many Rac GEFs. However, a previous study indicates that DOCK1 is recruited to the circular ruffle membrane through the interaction with phosphatidic acid and critically regulates its formation (Sanematsu et al., 2013). Because circular ruffle formation is important for both macropinocytosis and invasion (Buccione et al., 2004; Hoon et al., 2012), this feature might make DOCK1 a special GEF that links Rac activation to these cellular functions.

Although the expression patterns of DOCK1 and DOCK2 are strikingly different, these DOCK proteins are structurally related and act as Rac-specific GEFs (Kulkarni et al., 2011; Laurin and Côté, 2014). DOCK2 plays key roles in migration and activation of leukocytes (Fukui et al., 2001; Gotoh et al., 2008, 2010; Kunisaki et al., 2006; Nishikimi et al., 2009; Sanui et al., 2003), and its deficiency in humans causes severe infections (Dobbs et al., 2015). Therefore, for cancer therapy, it is essential to develop DOCK1-selective inhibitors. In this study, we initially identified FDOPP as a small-molecule inhibitor that preferentially suppresses DOCK1-mediated Rac activation. Structure-activity relationship studies clarified the importance of the sulfonamide fragment and two hydrophobic aromatic rings for its inhibitory activity. We successfully modified the structure of FDOPP into simplified biphenyl compound **6**, which showed higher DOCK1 selectivity than FDOPP. We assumed that the fine-tuning of two aromatic rings in compound **6** is a key to find DOCK1-selective inhibitors. Thus, we screened *p*-, *o*-, and *m*-substituted analogs (compounds **9**–**17**) and found that TBOPP (compound **16**) bearing the hydrophobic CF_3 group at the *m* position shows good DOCK1 selectivity. In contrast, hydrophilic substituent at the *m* position in compound **17** showed less potency, suggesting the existence of an additional hydrophobic region around the *m* position. Therefore, additional derivatives, compounds **18**–**22**, with other hydrophobic groups at the *m* position were screened. Compounds **19** and **20** inhibited the Rac GEF activity of DOCK1 with comparable potency to that of TBOPP, but DOCK1 selectivity decreased. Compounds **21** and **22** bearing the *m*-CF_3 group and additional substituent at either the *m* or the *p* position resulted in decreasing not only inhibitory activity but also DOCK1 selectivity. Thus, TBOPP was selected for further evaluation.

In this study, we have shown that TBOPP inhibits DOCK1-mediated Rac activation with a half-maximal inhibitory concentration (IC_{50}) of 8.4 μM, without affecting the Rac GEF activity of Trio and Tiam1. This IC_{50} value for DOCK1 was 8.7-fold and 5.4-fold lower than those for DOCK2 and DOCK5, respectively. The DOCK1 selectivity was confirmed by SPR-based binding assays and pull-down assays. More importantly, TBOPP did not impair the biological functions of DOCK2 and DOCK5 in functional assays. The precise mechanism of how TBOPP distinguishes DOCK1 and DOCK2 or DOCK5 remains to be determined. However, we found that the inhibitory activity of TBOPP was significantly reduced by mutating asparagine at position 1,540 of DOCK1 DHR-2 to lysine of the DOCK2 type (N1540K) (Figure S7), suggesting that this amino acid residue is involved in the interaction with TBOPP. Although the efficacy of TBOPP is somewhat limited in vitro, treatment of the Ras-transformed cancer cell lines, 3LL, HT1080, and DLD-1, with TBOPP dampened invasion, macropinocytosis, and survival under the condition of glutamine deprivation, in agreement with the genetic data. In addition, metastasis and growth of these Ras-transformed cancer cells were significantly suppressed in vivo when mice were treated with TBOPP. It is known that DOCK1 acts downstream of oncogenic RTKs and regulates invasion and metastasis of several cancer cells (Feng et al., 2011, 2012; Laurin et al., 2013). Therefore, the use of TBOPP would not be limited to cancers driven by oncogenic Ras but may also have potential benefits for broader types of tumors. We expect that TBOPP could be an excellent starting point for the development of DOCK1-targeting anti-cancer therapeutics with orders-of-magnitude higher efficacy and specificity by the pharmaceutical industry.

EXPERIMENTAL PROCEDURES

Animals

Dock1$^{flox/flox}$ mice have been described previously (Laurin et al., 2008, 2013). C57BL/6 mice and BALB/c nude mice were purchased from Japan Clea. These mice were maintained under specific pathogen-free conditions in the animal facility of Kyushu University. The protocol of animal experiments was approved by the committee of Ethics of Animal Experiments, Kyushu University.

In Silico Screening

Ligand-based and structure-based approaches for drug design (LBDD and SBDD, respectively) were employed to screen 202,789 compounds of the chemical library from the Platform for Drug Discovery, Informatics, and Structural Life Science (The University of Tokyo). See the Supplemental Experimental Procedures and Figure S4 for details.

Chemical Compounds

A total of 567 compounds used for wet laboratory screening were obtained from the Platform for Drug Discovery, Informatics, and Structural Life Science (The University of Tokyo). The synthesis and purification of each compound are described in Supplemental Experimental Procedures. All compounds were dissolved in DMSO and diluted with appropriate buffers immediately before use. The percentage of DMSO used for cellular assays was 0.2%.

In Vitro GEF Assays

Fluorescent GEF assays were performed as described previously (Nishikimi et al., 2012). The assays consisted of GST-Rac1 (10 μM), Bodipy-FL GTP (2.4 μM; Invitrogen G12411), and GEF proteins (0.05 μM for DOCK1, 0.1 μM

Figure 5. Structure-Activity Relationship of FDOPP, TBOPP, and Their Analogs

IC_{50} value (in micromolars) of each compound is shown for the Rac GEF activity of DOCK1 (D1), DOCK2 (D2), and DOCK5 (D5). The estimate of DOCK1 selectivity was obtained by dividing the IC_{50} value for DOCK2 or DOCK5 by that for DOCK1 and is described in the parentheses.
See also Figures S5 and S7.

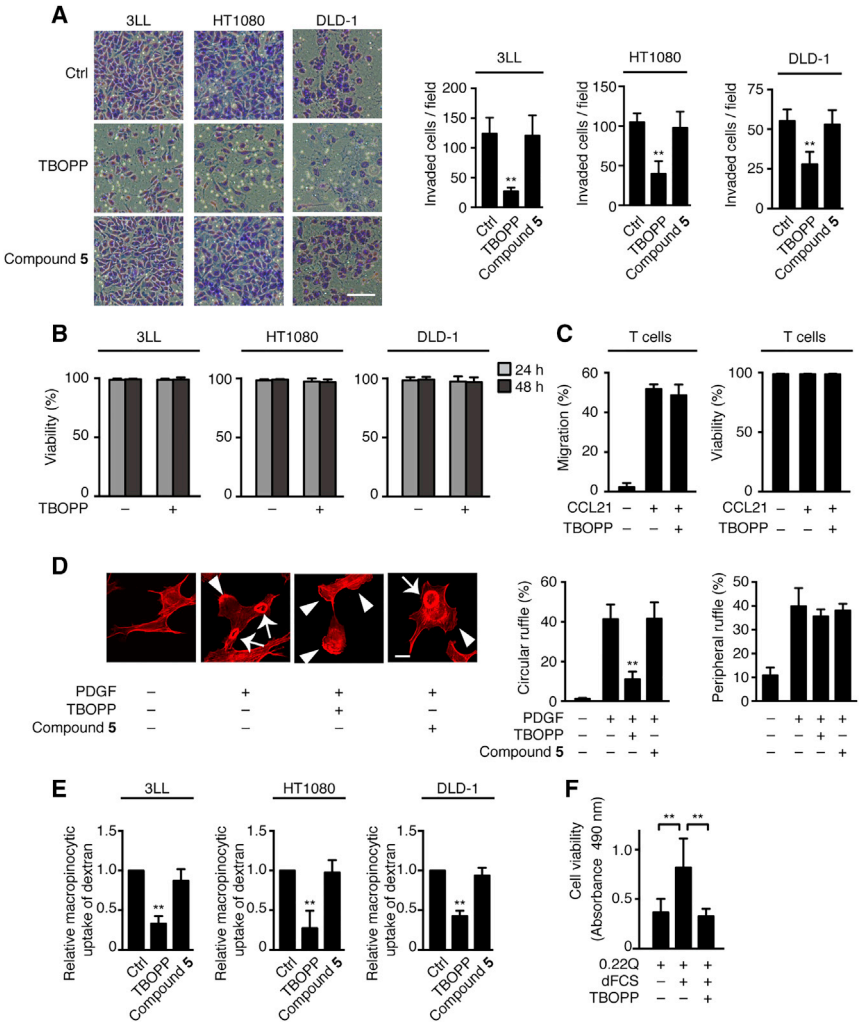

Figure 6. TBOPP Selectively Inhibits DOCK1-Dependent Cellular Functions

(A) Comparison of invasive activity of 3LL, HT1080, and DLD-1 cells with or without TBOPP treatment (12.5 μM). In each experiment, the number of invaded cells per field was determined by counting cells in four distinct fields. Scale bar, 100 μm. Data are expressed as mean ± SD of five independent experiments. **p < 0.01 compared with Ctrl samples treated with vehicle alone (ANOVA followed by Dunnett's post hoc test).

(B) No effect of TBOPP (12.5 μM) on the viability of 3LL, HT1080, and DLD-1 cells grown in complete DMEM. Cell viability was assessed by trypan blue exclusion. Data are expressed as mean ± SD of five (3LL and HT1080 cells) or three (DLD-1) independent experiments.

(C) No effect of TBOPP treatment (12.5 μM) on CCL21-induced T cell migration. Data are expressed as mean ± SD of five independent experiments.

(D) Inhibition of PDGF-induced circular, but not peripheral, ruffle formation in MEFs by TBOPP treatment (12.5 μM). Arrowheads and arrows indicate peripheral ruffles and circular ruffles, respectively. Scale bar, 50 μm. In each experiment, at least 80 cells were analyzed. Data are collected from five independent experiments and expressed as mean ± SD of the percentage of the cells with circular or peripheral ruffles. **p < 0.01 compared with vehicle-treated samples with PDGF stimulation (ANOVA followed by Dunnett's post hoc test).

(E) Comparison of macropinocytic uptake of dextran in 3LL, HT1080, and DLD-1 cells with or without TBOPP treatment (12.5 μM). Data (mean ± SD, n = 5) are expressed as the relative index after normalization of the level of Ctrl samples treated with vehicle alone to an arbitrary value of 1. **p < 0.01 compared with Ctrl samples (ANOVA followed by Dunnett's post hoc test).

(F) Effect of TBOPP treatment (12.5 μM) on viability of 3LL cells under the condition of glutamine deprivation (0.22Q) with or without dFCS addition. Data are expressed as mean ± SD of five independent experiments. **p < 0.01 (two-tailed unpaired Student's t test).

for DOCK2 and DOCK5, 1 μM for Trio, and 2 μM for Tiam1, depending on their GEF activities) in the reaction buffer (20 mM MES-NaOH, 150 mM NaCl, 10 mM $MgCl_2$, and 20 μM GDP [pH 7.0]). See the Supplemental Experimental Procedures for details.

SPR-Based Binding Assays

SPR-based binding assays were performed with a Biacore T200 instrument (GE Healthcare Life Sciences). For this purpose, His-SUMO-tagged DOCK1 DHR-2, DOCK2 DHR-2, or Tiam1 DH-PH protein was immobilized onto a CM5 Sensor Chip (approximately 8,000 response units (RUs), respectively) using an Amine Coupling Kit (GE Healthcare Life Sciences). Data were collected in HEPES-buffered saline (HBS) buffer (10 mM HEPES [pH 7.5] and 150 mM NaCl) containing 0.005% surfactant P-20 and 3% DMSO. Serial concentrations (0–120 μM) of TBOPP, compound **5**, or DMSO (blank) were injected, and response was measured. Data were analyzed by steady-state affinity analysis with five sample concentrations in triplicate using the manufacturer's software, and K_d and B_{max} were obtained using Prism 5 with the one site-specific binding model using the equation $y = B_{max} \times x/(K_d + x)$, where x or y indicates the concentration of TBOPP or the level of specific binding, respectively.

Pull-Down Assays and Immunoblotting

Rac activation assays were performed as previously described (Fukui et al., 2001). To examine the effect of TBOPP on the association between Rac1 and each Rac GEF, recombinant protein encoding His-SUMO-tagged DOCK1 DHR-2, DOCK2 DHR-2, and Tiam1 DH-PH (each 3 μg) was incubated with TBOPP (final 100 μM), compound **5**, or DMSO (2%) in 200 μL of binding buffer (20 mM MES-NaOH [pH 7.0], 150 mM NaCl, 2.5 mM EDTA, and 0.0001% Tween 20) before assays. Expression and activation of each signaling molecule were examined by immunoblotting. See Supplemental Experimental Procedures for details.

Invasion Assays

Cell invasive activity was measured by using BioCoat Matrigel invasion chambers (Corning) according to the protocol provided by the manufacturer. Briefly, cells (2.5×10^4 cells for MEFs and HT1080, 3.75×10^4 cells for DLD-1, and 7.5×10^4 cells for 3LL) were suspended in serum-free medium and loaded into the upper chamber with an 8 μm pore size membrane and a thin layer of Matrigel basement membrane matrix, which were placed onto 24-well plates containing DMEM-supplemented 5% FCS (MEFs) or 10% FCS (HT1080, 3LL, and DLD-1). Cells were allowed to migrate for 22 hr (MEFs, HT1080,

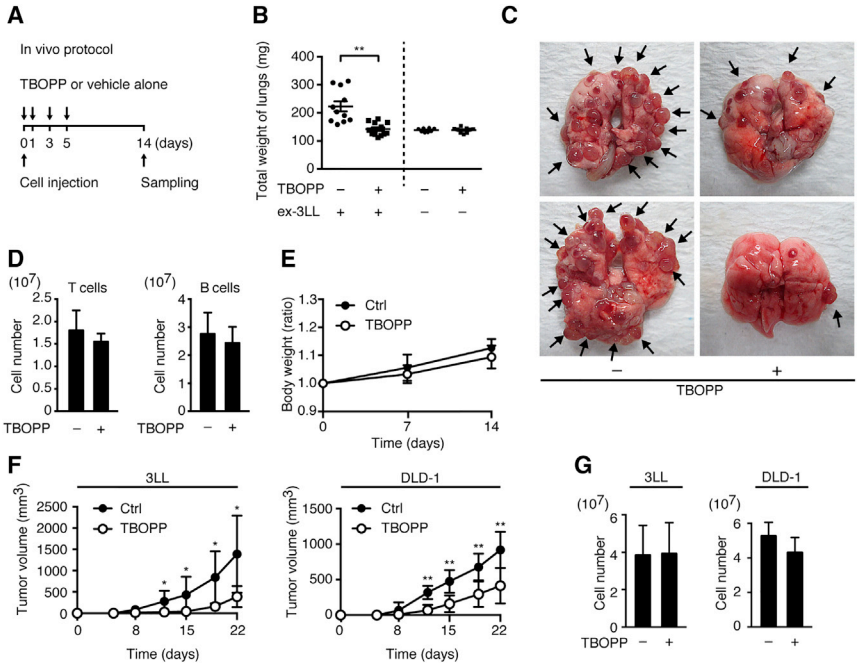

Figure 7. Treatment with TBOPP Suppresses Cancer Metastasis and Growth In Vivo

(A) Schematic illustration of the protocol used for TBOPP administration for in vivo metastasis assays (B and C).

(B) Effect of TBOPP treatment on lung metastasis of ex-3LL cells. Data (total weight of lungs) are expressed as mean ± SD of 11 mice (vehicle alone) or 12 mice (TBOPP) per group. **p < 0.01 (two-tailed unpaired Student's t test). As Ctrl, the lung weights of mice without inoculation of ex-3LL cells are indicated (n = 8 for vehicle alone; n = nine for TBOPP).

(C) Representative images of the lung from mice inoculated with ex-3LL cells with or without TBOPP treatment.

(D) Comparable numbers of T and B cells in the spleen of mice treated with or without TBOPP, as in (A). Data are expressed as mean ± SD of eight mice (vehicle alone) or nine mice (TBOPP).

(E) No effect of TBOPP on body weight during TBOPP treatment. Data are expressed as mean ± SD of eight mice (vehicle alone; Ctrl) or nine mice (TBOPP).

(F) Effect of TBOPP treatment on in vivo growth of 3LL and DLD-1 cells. After inoculation of 3LL or DLD-1 cells into the back of BALB/c nude mice, TBOPP was continuously injected into mice using an implantable and programmable microfusion pump system. Data are expressed as mean ± SD of six mice per group. *p < 0.05, **p < 0.01 (two-tailed unpaired Student's t test).

(G) Comparable B cell numbers in the spleen from mice inoculated with 3LL or DLD-1 cells in the presence or absence of TBOPP treatment. Data are expressed as mean ± SD of six mice per group.

and 3LL) or 28 hr (DLD-1) at 37°C and were stained with DAPI (Dojindo Laboratories) or Diff Quick (Sysmex). Samples were analyzed with a laser scanning confocal microscope (LSM 510 Meta; Zeiss) or an inverted light microscope (IX70; Olympus).

Macropinocytosis Assays

Macropinocytosis was assessed by measuring the cellular uptake of tetramethyl rhodamine (TMR)-labeled dextran (Invitrogen). For this purpose, cells were seeded on fibronectin-coated glass-bottom dishes (Matsunami) for 24–48 hr. After starvation for 18 hr, cells were incubated for 1 hr (MEFs, HT1080, and 3LL) or 4 hr (DLD-1) at 37°C with complete DMEM containing TMR-dextran at a final concentration of 0.25 mg/mL. At the end of the incubation period, cells were rinsed three times with cold PBS and immediately fixed in 4% paraformaldehyde before staining with DAPI. Samples were analyzed with a laser scanning confocal microscope (LSM 510 Meta).

Glutamine Deprivation Assays

Glutamine-free DMEM (Life Technologies) was supplemented to the specified concentration of glutamine in the presence of 5% dFCS and 25 mM HEPES (Sigma-Aldrich). Cells were plated in a 96-well plate at a density of 1,000 cells per well. Then, 32 hr after seeding, cells were rinsed with PBS and incubated in the glutamine-deprivation medium. After 3 days of the culture, cell viability was assessed with the CytoTox 96 non-radioactive cytotoxicity assay kit (Promega). In all experiments, medium was replaced every 24 hr.

In Vivo Metastasis Assay and Tumor Growth Assay

For in vivo metastasis assay, ex-3LL cells (1×10^6 cells per mouse) were injected into the tail vein of 6- to 8-week-old C57BL/6 mice. TBOPP was dissolved in PBS containing 12.5% Cremophol EL (Calbiochem) and 12.5% ethanol and was administrated to mice on days 0, 1, 3, and 5 at 0.67 mg per mouse. After 2 weeks, mice were sacrificed, and the lungs were removed to measure weight.

To examine the effect of TBOPP on tumor growth in mice, TBOPP was dissolved as described above at 1 mg/300 μL and injected using an implantable and programmable microfusion pump system (iPRECIO Micro Infusion Pump System, SMP-300; Primetech Corporation). For this purpose, the catheter part of the microinfusion pump was inserted into the left external jugular vein via midcervical incision, and the main body of the microinfusion pump was implanted subcutaneously in the lumber region. After inoculation of 3LL or DLD-1 cells into the back of 8-week-old BALB/c nude mice on day 0, TBOPP or vehicle was continuously injected into mice at 0.7 μL/hr. Mice were sacrificed on day 22, and the size of the resulting tumors was determined as follows: $V = \pi/6 \times \sqrt{(\text{length} \times \text{width})^3}$.

Statistical Analysis

Differences between groups were compared using two-tailed unpaired Student's t test (two groups) or one-way ANOVA (multiple groups) followed by Dunnett's post hoc test. Error bars denote SD.

SUPPLEMENTAL INFORMATION

Supplemental Information includes Supplemental Experimental Procedures and seven figures and can be found with this article online at http://dx.doi.org/10.1016/j.celrep.2017.04.016.

AUTHOR CONTRIBUTIONS

H.T., T.U., M.W., M.U., F.S., M.K.-N., and T.T. performed functional and biochemical analyses; T.S., S.M., K.O., and M.K. synthesized compounds; D.T., M.K.-N., T.H., and S.Y. performed in silico screening; D.S. and D.K. did metabolite analyses; J.-F.C., S.S., E.O., and Y.M. interpreted the data and provided reagents; H.T., T.U., M.K.-N., T.S., D.T., S.M., T.H., Y.M., J.-F.C., and S.Y. contributed to writing the manuscript; and Y.F. conceived the project, interpreted the data, and wrote the manuscript.

ACKNOWLEDGMENTS

We thank A. Inayoshi, A. Aosaka, and C. Mishima-Tsumagari for technical assistance. This research is supported by the Leading Advanced Projects for Medical Innovation (LEAP) from Japan Agency for Medical Research and Development (AMED, to Y.F.); the Project for Development of Innovative Research on Cancer Therapeutics (P-Direct) from AMED (to Y.F.); Grants-in-Aid for Scientific Research from the Japan Society for the Promotion of Science (25251015 to Y.F. and 15K06987 to M.K.-N.); Center for Clinical and Translational Research of Kyushu University (to Y.F.); the Takeda Science Foundation (to F.S.); and the Canadian Institute for Health Research (MOP-144425 to J.-F.C.). J.-F.C. holds a Senior FRQS career award.

Received: September 5, 2016
Revised: February 2, 2017
Accepted: April 5, 2017
Published: May 2, 2017

REFERENCES

Buccione, R., Orth, J.D., and McNiven, M.A. (2004). Foot and mouth: podosomes, invadopodia and circular dorsal ruffles. Nat. Rev. Mol. Cell Biol. *5*, 647–657.

Colicelli, J. (2004). Human RAS superfamily proteins and related GTPases. Sci. STKE *2004*, RE13.

Commisso, C., Davidson, S.M., Soydaner-Azeloglu, R.G., Parker, S.J., Kamphorst, J.J., Hackett, S., Grabocka, E., Nofal, M., Drebin, J.A., Thompson, C.B., et al. (2013). Macropinocytosis of protein is an amino acid supply route in Ras-transformed cells. Nature *497*, 633–637.

Cox, A.D., Fesik, S.W., Kimmelman, A.C., Luo, J., and Der, C.J. (2014). Drugging the undruggable RAS: mission possible? Nat. Rev. Drug Discov. *13*, 828–851.

Dobbs, K., Domínguez Conde, C., Zhang, S.Y., Parolini, S., Audry, M., Chou, J., Haapaniemi, E., Keles, S., Bilic, I., Okada, S., et al. (2015). Inherited DOCK2 deficiency in patients with early-onset invasive infections. N. Engl. J. Med. *372*, 2409–2422.

Feng, H., Hu, B., Liu, K.W., Li, Y., Lu, X., Cheng, T., Yiin, J.J., Lu, S., Keezer, S., Fenton, T., et al. (2011). Activation of Rac1 by Src-dependent phosphorylation of Dock180(^{Y1811}) mediates PDGFRα-stimulated glioma tumorigenesis in mice and humans. J. Clin. Invest. *121*, 4670–4684.

Feng, H., Hu, B., Jarzynka, M.J., Li, Y., Keezer, S., Johns, T.G., Tang, C.K., Hamilton, R.L., Vuori, K., Nishikawa, R., et al. (2012). Phosphorylation of dedicator of cytokinesis 1 (Dock180) at tyrosine residue Y722 by Src family kinases mediates EGFRvIII-driven glioblastoma tumorigenesis. Proc. Natl. Acad. Sci. USA *109*, 3018–3023.

Fukui, Y., Hashimoto, O., Sanui, T., Oono, T., Koga, H., Abe, M., Inayoshi, A., Noda, M., Oike, M., Shirai, T., and Sasazuki, T. (2001). Haematopoietic cell-specific CDM family protein DOCK2 is essential for lymphocyte migration. Nature *412*, 826–831.

Gaglio, D., Soldati, C., Vanoni, M., Alberghina, L., and Chiaradonna, F. (2009). Glutamine deprivation induces abortive s-phase rescued by deoxyribonucleotides in k-ras transformed fibroblasts. PLoS ONE *4*, e4715.

Gotoh, K., Tanaka, Y., Nishikimi, A., Inayoshi, A., Enjoji, M., Takayanagi, R., Sasazuki, T., and Fukui, Y. (2008). Differential requirement for DOCK2 in migration of plasmacytoid dendritic cells versus myeloid dendritic cells. Blood *111*, 2973–2976.

Gotoh, K., Tanaka, Y., Nishikimi, A., Nakamura, R., Yamada, H., Maeda, N., Ishikawa, T., Hoshino, K., Uruno, T., Cao, Q., et al. (2010). Selective control of type I IFN induction by the Rac activator DOCK2 during TLR-mediated plasmacytoid dendritic cell activation. J. Exp. Med. *207*, 721–730.

Grimsley, C.M., Kinchen, J.M., Tosello-Trampont, A.C., Brugnera, E., Haney, L.B., Lu, M., Chen, Q., Klingele, D., Hengartner, M.O., and Ravichandran, K.S. (2004). Dock180 and ELMO1 proteins cooperate to promote evolutionarily conserved Rac-dependent cell migration. J. Biol. Chem. *279*, 6087–6097.

Gumienny, T.L., Brugnera, E., Tosello-Trampont, A.C., Kinchen, J.M., Haney, L.B., Nishiwaki, K., Walk, S.F., Nemergut, M.E., Macara, I.G., Francis, R., et al. (2001). CED-12/ELMO, a novel member of the CrkII/Dock180/Rac pathway, is required for phagocytosis and cell migration. Cell *107*, 27–41.

Heid, I., Lubeseder-Martellato, C., Sipos, B., Mazur, P.K., Lesina, M., Schmid, R.M., and Siveke, J.T. (2011). Early requirement of Rac1 in a mouse model of pancreatic cancer. Gastroenterology *141*, 719–730, 730.e1–730.e7.

Hoon, J.L., Wong, W.K., and Koh, C.G. (2012). Functions and regulation of circular dorsal ruffles. Mol. Cell. Biol. *32*, 4246–4257.

Jarzynka, M.J., Hu, B., Hui, K.M., Bar-Joseph, I., Gu, W., Hirose, T., Haney, L.B., Ravichandran, K.S., Nishikawa, R., and Cheng, S.Y. (2007). ELMO1 and Dock180, a bipartite Rac1 guanine nucleotide exchange factor, promote human glioma cell invasion. Cancer Res. *67*, 7203–7211.

Kawazu, M., Ueno, T., Kontani, K., Ogita, Y., Ando, M., Fukumura, K., Yamato, A., Soda, M., Takeuchi, K., Miki, Y., et al. (2013). Transforming mutations of RAC guanosine triphosphatases in human cancers. Proc. Natl. Acad. Sci. USA *110*, 3029–3034.

Kissil, J.L., Walmsley, M.J., Hanlon, L., Haigis, K.M., Bender Kim, C.F., Sweet-Cordero, A., Eckman, M.S., Tuveson, D.A., Capobianco, A.J., Tybulewicz, V.L.J., and Jacks, T. (2007). Requirement for Rac1 in a K-ras induced lung cancer in the mouse. Cancer Res. *67*, 8089–8094.

Kulkarni, K., Yang, J., Zhang, Z., and Barford, D. (2011). Multiple factors confer specific Cdc42 and Rac protein activation by dedicator of cytokinesis (DOCK) nucleotide exchange factors. J. Biol. Chem. *286*, 25341–25351.

Kunisaki, Y., Nishikimi, A., Tanaka, Y., Takii, R., Noda, M., Inayoshi, A., Watanabe, K., Sanematsu, F., Sasazuki, T., Sasaki, T., and Fukui, Y. (2006). DOCK2 is a Rac activator that regulates motility and polarity during neutrophil chemotaxis. J. Cell Biol. *174*, 647–652.

Lanzetti, L., Palamidessi, A., Areces, L., Scita, G., and Di Fiore, P.P. (2004). Rab5 is a signalling GTPase involved in actin remodelling by receptor tyrosine kinases. Nature *429*, 309–314.

Laurin, M., and Côté, J.F. (2014). Insights into the biological functions of Dock family guanine nucleotide exchange factors. Genes Dev. *28*, 533–547.

Laurin, M., Fradet, N., Blangy, A., Hall, A., Vuori, K., and Côté, J.F. (2008). The atypical Rac activator Dock180 (Dock1) regulates myoblast fusion in vivo. Proc. Natl. Acad. Sci. USA *105*, 15446–15451.

Laurin, M., Huber, J., Pelletier, A., Houalla, T., Park, M., Fukui, Y., Haibe-Kains, B., Muller, W.J., and Côté, J.F. (2013). Rac-specific guanine nucleotide exchange factor DOCK1 is a critical regulator of HER2-mediated breast cancer metastasis. Proc. Natl. Acad. Sci. USA *110*, 7434–7439.

Li, X., Gao, X., Liu, G., Xiong, W., Wu, J., and Rao, Y. (2008). Netrin signal transduction and the guanine nucleotide exchange factor DOCK180 in attractive signaling. Nat. Neurosci. *11*, 28–35.

Malliri, A., van der Kammen, R.A., Clark, K., van der Valk, M., Michiels, F., and Collard, J.G. (2002). Mice deficient in the Rac activator Tiam1 are resistant to Ras-induced skin tumours. Nature *417*, 867–871.

Nishikimi, A., Fukuhara, H., Su, W., Hongu, T., Takasuga, S., Mihara, H., Cao, Q., Sanematsu, F., Kanai, M., Hasegawa, H., et al. (2009). Sequential regulation of DOCK2 dynamics by two phospholipids during neutrophil chemotaxis. Science *324*, 384–387.

Nishikimi, A., Uruno, T., Duan, X., Cao, Q., Okamura, Y., Saitoh, T., Saito, N., Sakaoka, S., Du, Y., Suenaga, A., et al. (2012). Blockade of inflammatory responses by a small-molecule inhibitor of the Rac activator DOCK2. Chem. Biol. *19*, 488–497.

Prior, I.A., Lewis, P.D., and Mattos, C. (2012). A comprehensive survey of Ras mutations in cancer. Cancer Res. *72*, 2457–2467.

Qiu, R.G., Chen, J., Kirn, D., McCormick, F., and Symons, M. (1995). An essential role for Rac in Ras transformation. Nature *374*, 457–459.

Robinson, M.M., McBryant, S.J., Tsukamoto, T., Rojas, C., Ferraris, D.V., Hamilton, S.K., Hansen, J.C., and Curthoys, N.P. (2007). Novel mechanism of inhibition of rat kidney-type glutaminase by bis-2-(5-phenylacetamido-1,2,4-thiadiazol-2-yl)ethyl sulfide (BPTES). Biochem. J. *406*, 407–414.

Sahai, E., and Marshall, C.J. (2002). RHO-GTPases and cancer. Nat. Rev. Cancer *2*, 133–142.

Sanematsu, F., Hirashima, M., Laurin, M., Takii, R., Nishikimi, A., Kitajima, K., Ding, G., Noda, M., Murata, Y., Tanaka, Y., et al. (2010). DOCK180 is a Rac activator that regulates cardiovascular development by acting downstream of CXCR4. Circ. Res. *107*, 1102–1105.

Sanematsu, F., Nishikimi, A., Watanabe, M., Hongu, T., Tanaka, Y., Kanaho, Y., Côté, J.F., and Fukui, Y. (2013). Phosphatidic acid-dependent recruitment and function of the Rac activator DOCK1 during dorsal ruffle formation. J. Biol. Chem. *288*, 8092–8100.

Sanui, T., Inayoshi, A., Noda, M., Iwata, E., Oike, M., Sasazuki, T., and Fukui, Y. (2003). DOCK2 is essential for antigen-induced translocation of TCR and lipid rafts, but not PKC-θ and LFA-1, in T cells. Immunity *19*, 119–129.

Schmidt, A., and Hall, A. (2002). Guanine nucleotide exchange factors for Rho GTPases: turning on the switch. Genes Dev. *16*, 1587–1609.

Shirasawa, S., Furuse, M., Yokoyama, N., and Sasazuki, T. (1993). Altered growth of human colon cancer cell lines disrupted at activated Ki-ras. Science *260*, 85–88.

Spiegel, J., Cromm, P.M., Zimmermann, G., Grossmann, T.N., and Waldmann, H. (2014). Small-molecule modulation of Ras signaling. Nat. Chem. Biol. *10*, 613–622.

Suetsugu, S., Yamazaki, D., Kurisu, S., and Takenawa, T. (2003). Differential roles of WAVE1 and WAVE2 in dorsal and peripheral ruffle formation for fibroblast cell migration. Dev. Cell *5*, 595–609.

Van Aelst, L., and D'Souza-Schorey, C. (1997). Rho GTPases and signaling networks. Genes Dev. *11*, 2295–2322.

Wang, H., Linghu, H., Wang, J., Che, Y.L., Xiang, T.X., Tang, W.X., and Yao, Z.W. (2010). The role of Crk/Dock180/Rac1 pathway in the malignant behavior of human ovarian cancer cell SKOV3. Tumour Biol. *31*, 59–67.

White, E. (2013). Exploiting the bad eating habits of Ras-driven cancers. Genes Dev. *27*, 2065–2071.

Wu, M.C., Arimura, G.K., and Yunis, A.A. (1978). Mechanism of sensitivity of cultured pancreatic carcinoma to asparaginase. Int. J. Cancer *22*, 728–733.

Ying, H., Kimmelman, A.C., Lyssiotis, C.A., Hua, S., Chu, G.C., Fletcher-Sananikone, E., Locasale, J.W., Son, J., Zhang, H., Coloff, J.L., et al. (2012). Oncogenic Kras maintains pancreatic tumors through regulation of anabolic glucose metabolism. Cell *149*, 656–670.

Zhao, F., Siu, M.K.Y., Jiang, L., Tam, K.F., Ngan, H.Y.S., Le, X.F., Wong, O.G.W., Wong, E.S.Y., Chan, H.Y., and Cheung, A.N.Y. (2011). Overexpression of dedicator of cytokinesis I (Dock180) in ovarian cancer correlated with aggressive phenotype and poor patient survival. Histopathology *59*, 1163–1172.

Zwartkruis, F.J.T., and Burgering, B.M.T. (2013). Ras and macropinocytosis: trick and treat. Cell Res. *23*, 982–983.

Cell Reports, Volume *19*

Supplemental Information

Targeting Ras-Driven Cancer Cell Survival and Invasion through Selective Inhibition of DOCK1

Hirotada Tajiri, Takehito Uruno, Takahiro Shirai, Daisuke Takaya, Shigeki Matsunaga, Daiki Setoyama, Mayuki Watanabe, Mutsuko Kukimoto-Niino, Kounosuke Oisaki, Miho Ushijima, Fumiyuki Sanematsu, Teruki Honma, Takaho Terada, Eiji Oki, Senji Shirasawa, Yoshihiko Maehara, Dongchon Kang, Jean-François Côté, Shigeyuki Yokoyama, Motomu Kanai, and Yoshinori Fukui

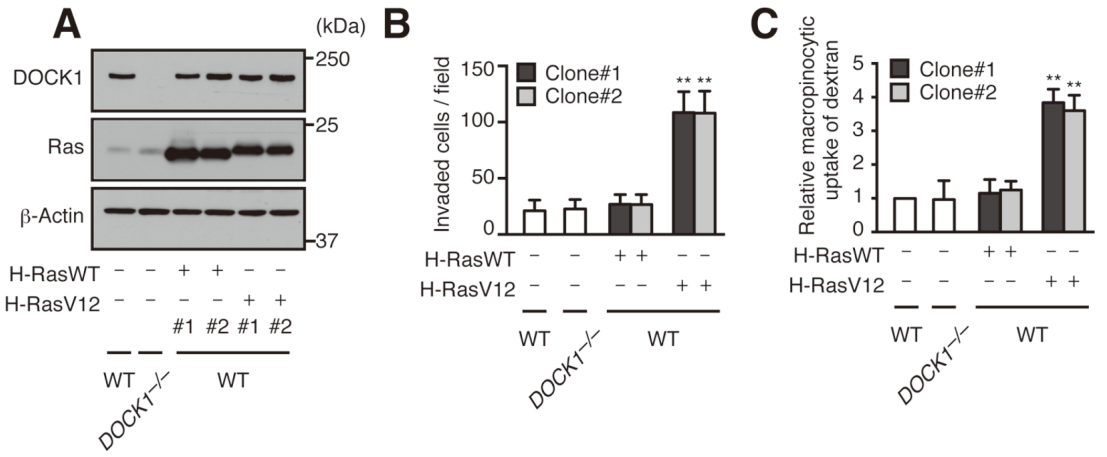

Figure S1. Overexpression of WT Ras in MEFs Affects Neither Invasion nor Macropinocytosis, Related to Figure 1.

(A) Western blot analysis for the expression of DOCK1 and Ras in WT MEFs with exogenous WT H-Ras (H-RasWT) or H-RasV12 expression. The numerals (#) indicate the clone number.

(B) Comparison of invasive activity among WT MEFs expressing H-RasWT or H-RasV12. In each experiment, the number of invaded cells per field was determined by counting cells in four distinct fields. Data are expressed as mean ± SD of five independent experiments. **$p < 0.01$ compared with WT samples without exogenous Ras expression (ANOVA followed by Dunnett's post hoc test).

(C) Comparison of macropinocytic uptake of dextran among WT MEFs with H-RasWT or H-RasV12 expression. Data (mean ± SD, n = 5) are expressed as the relative index after normalization (WT level without exogenous Ras expression to an arbitrary value of 1). **$p < 0.01$ compared with WT samples without exogenous Ras expression (ANOVA followed by Dunnett's post hoc test).

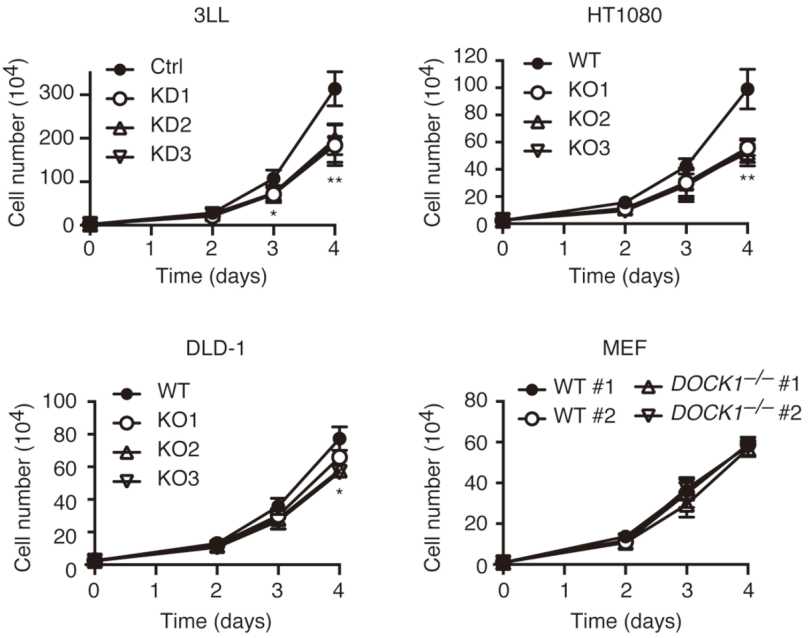

Figure S2. Proliferation of Ras-Transformed Cells Is Only Modestly Affected in the Absence of DOCK1 under Normal Culture Condition, Related to Figure 2.

Comparison of in vitro proliferation among 3LL-KD, HT1080-KO, DLD-1-KO, *Dock1*$^{-/-}$ H-RasV12-expressing-MEFs and their parent or control (Ctrl) cells. The numerals indicate the clone number. Data are expressed as mean ± SD of five (3LL and H-RasV12-expressing-MEFs) or three (HT1080 and DLD-1) independent experiments. *$p < 0.05$, **$p < 0.01$ compared with control or WT samples (ANOVA followed by Dunnett's post hoc test).

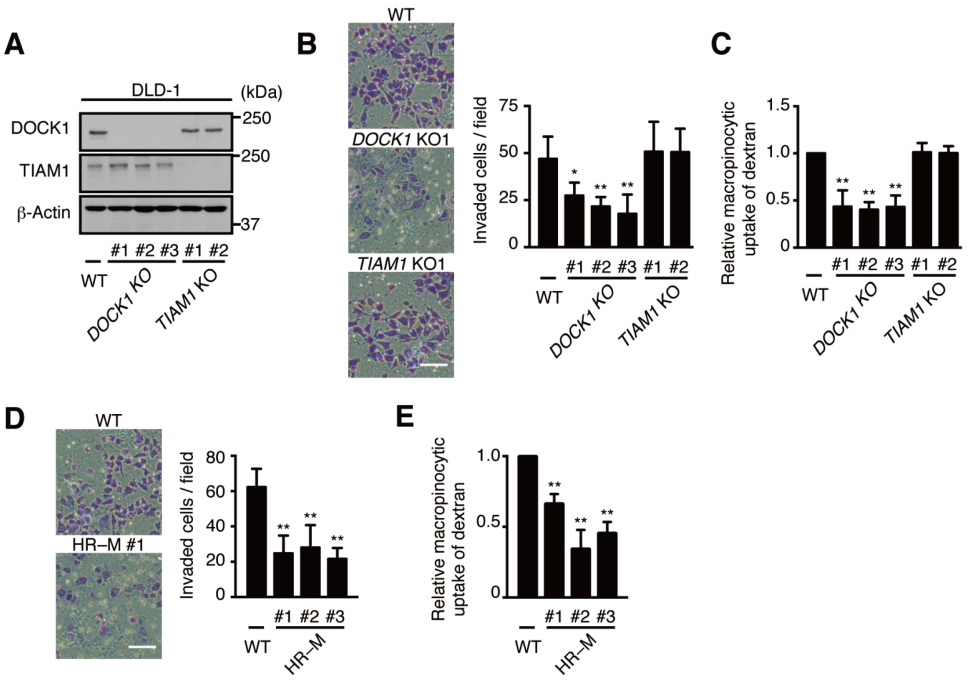

Figure S3. Effect of Deficiency of TIAM1 or Oncogenic Ras on Invasion and Macropinocytosis of Cancer Cells, Related to Figure 2.

(A) Western blot analysis for the expression of DOCK1 and TIAM1 in DLD-1 cells lacking DOCK1 (DOCK1-KO) or TIAM1 (TIAM1-KO). The numerals (#) indicate the clone number.

(B) Comparison of invasive activity among DOCK1-KO, TIAM1-KO and their parent cells. In each experiment, the number of invaded cells per field was determined by counting cells in four distinct fields. Scale bar, 100 μm. Data are expressed as mean ± SD of five independent experiments. *$p < 0.05$, **$p < 0.01$ compared with WT sample (ANOVA followed by Dunnett's post hoc test).

(C) Comparison of macropinocytic uptake of dextran among DOCK1-KO, TIAM1-KO and their parent cells. Data (mean ± SD, n = 5) are expressed as the relative index after normalization of WT level to an arbitrary value of 1. **$p < 0.01$ compared with WT samples (ANOVA followed by Dunnett's post hoc test).

(D) Comparison of invasive activity among DLD-1 HR-M (clones #1-#3) and their parent cells. In each experiment, the number of invaded cells per field was determined by counting cells in four distinct fields. Scale bar, 100 μm. Data are expressed as mean ± SD of five independent experiments. **$p < 0.01$ compared with WT sample (ANOVA followed by Dunnett's post hoc test).

(E) Comparison of macropinocytic uptake of dextran among DLD-1 HR-M (clones #1-#3) and their parent cells. Data (mean ± SD, n = 5) are expressed as the relative index after normalization of WT level to an arbitrary value of 1. **$p < 0.01$ compared with WT samples (ANOVA followed by Dunnett's post hoc test).

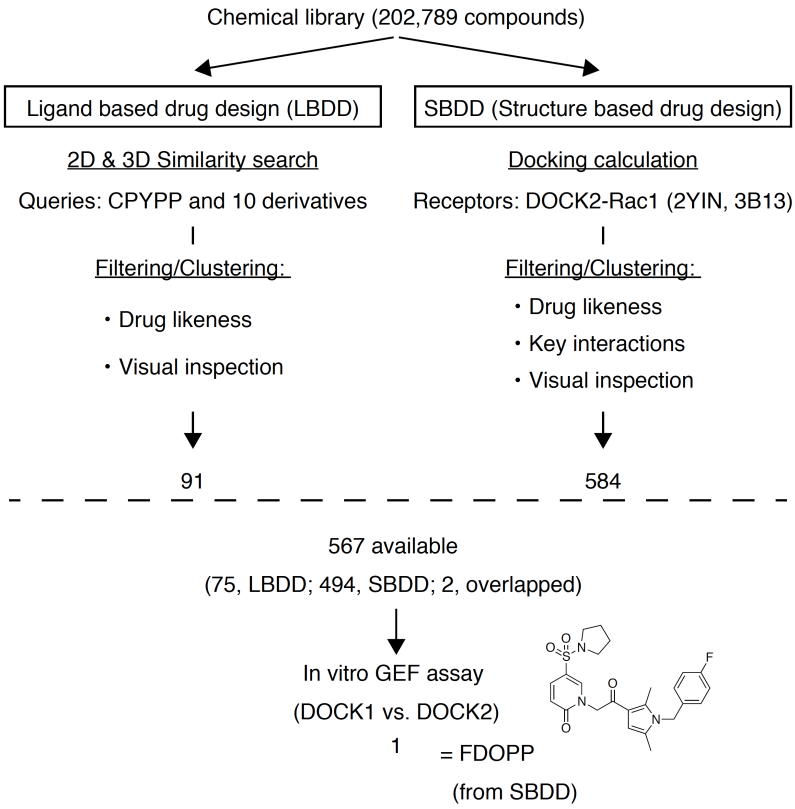

Figure S4. Strategy Used for In Silico and Wet Laboratory Screening for Development of DOCK1-Selective Inhibitors, Related to Figure 4.

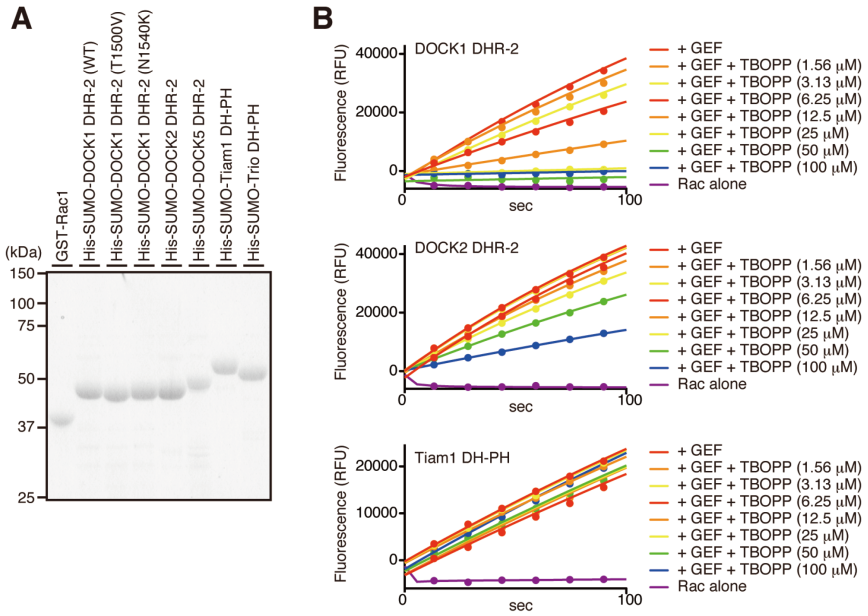

Figure S5. Fluorescent In Vitro GEF Assays Showing the Effect of TBOPP on the Rac GEF Activity of DOCK1, DOCK2 and Tiam1, Related to Figure 4 and Figure 5.

(A) Recombinant proteins used in this study. Five μg of each protein was separated on a 10% SDS-PAGE gel and stained with Coomassie Brilliant Blue.

(B) Time course showing the GEF-mediated loading of the fluorescent GTP on Rac and the effect of TBOPP treatment. Data are representative of three or four independent experiments.

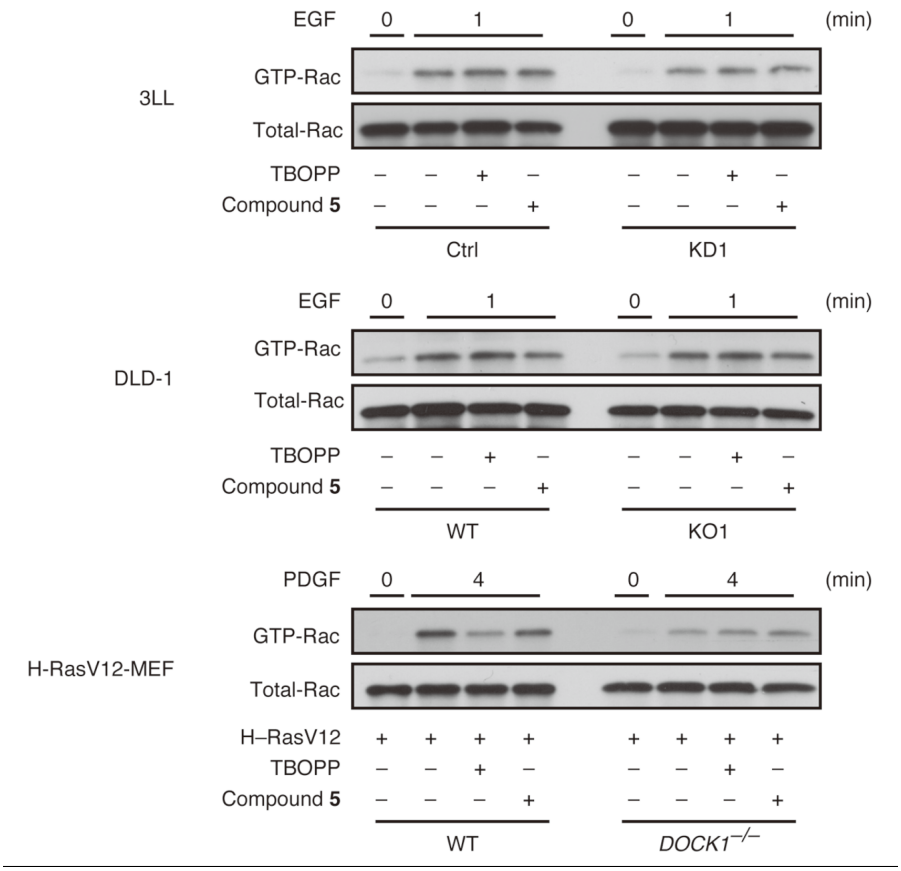

Figure S6. Effect of TBOPP on EGF- or PDGF-Induced Rac Activation in Ras-Transformed Cells with or without DOCK1 Expression, Related to Figure 4.

Following treatment of cells with TBOPP or compound **5** (50 μM), EGF- or PDGF-induced Rac activation was analyzed by pull-down assays.

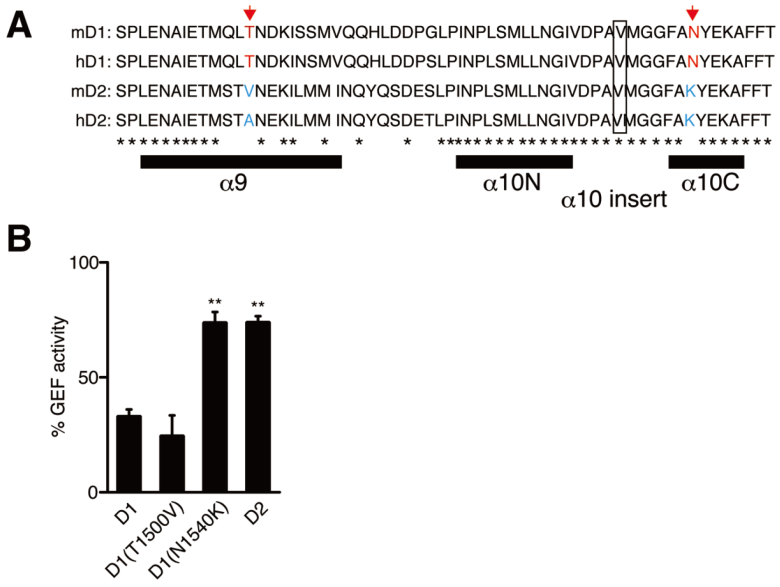

Figure S7. Possible Involvement of Asparagine at Position 1,540 of DOCK1 DHR-2 Domain in Interaction with TBOPP, Related to Figure 4 and Figure 5.

(A) Comparison of the amino acid sequences of mouse (m) and human (h) DOCK1 (D1) and DOCK2 (D2) DHR-2 domains. The nucleotide sensor (valine) is indicated by a box. Two amino acid residues used for mutation experiments are highlighted in red or blue.

(B) Effect of the amino acid substitution of DOCK1 DHR-2 domain (T1500V or N1540K) on the inhibitory activity of TBOPP (12.5 μM). As controls, WT DOCK1 (D1) or DOCK2 (D2) DHR-2 samples were simultaneously analyzed. Data are expressed as mean ± SD of five independent experiments after normalization of the value of control sample treated with vehicle alone as 100%. **p < 0.01 compared with the WT DOCK1 samples (ANOVA followed by Dunnett's post hoc test).

Supplemental Experimental Procedures

Cell Preparation and Culture

Primary MEFs were generated from E13.5 WT and *Dock1*$^{flox/flox}$ mice, and *Dock1* gene expression was deleted in the latter by expressing Cre recombinase, as previously described (Sanematsu et al., 2013). These MEFs were immortalized by transfection with a plasmid pCX4bsr-SV40ER before use. Immortalized MEFs were cultured in DMEM medium (Wako Pure Chemical Industries) supplemented with 10% heat-inactivated FCS (Nichirei Bioscience), 100 U/ml penicillin (Life Technologies) and 100 μg/ml streptomycin (Life Technologies) (designated complete DMEM medium). A mouse Lewis lung carcinoma cell line 3LL and its derivative ex-3LL with high metastatic property were obtained from Japanese Collection Research Bioresources (JCRB). A human sarcoma cell line HT1080 was provided by Y. Matsumoto (Kyushu University, Fukuoka, Japan), respectively. A human colon cancer cell line DLD-1 and its derivative DLD-1 HR-M have been described (Shirasawa et al., 1993). These cancer cell lines other than ex-3LL were maintained in complete D-MEM medium, and ex-3LL cells were maintained in RPMI 1640 medium (Wako Pure Chemical Industries) supplemented with 10% heat-inactivated FCS (Nichirei Bioscience), 100 U/ml penicillin (Life Technologies) and 100 μg/ml streptomycin (Life Technologies).

In Silico Screening

For LBDD, 2D and 3D similarity search was performed using the DOCK2 inhibitor CPYPP (Nishikimi et al., 2012) and its ten derivatives as queries. 3D coordinates of the queries and library compounds were generated by Omega (OpenEye Scientific Software Inc.) (Hawkins et al., 2010). In 2D similarity search, three 2D chemical fingerprints: MDL public key, ECFP4 and GpiDAPH3 were used as similarity measure. MDL public key and ECFP4 were calculated by Pipeline Pilot (Version 8.5; Dassault Systèmes BIOVIA, San Diego). GpiDAPH3 was calculated by MOE (Chemical Computing Group Inc., Montreal, Canada). For each similarity measure, normalized Tanimoto Coefficient (TC) (Flower, 1998) was used to rank compounds, and top 100 compounds were used. In 3D similarity search, ROCS (OpenEye Scientific Software Inc.) (Rush et al., 2005) was applied with Combo-Score of 1.4 or above as a cutoff. For SBDD, the crystal structures of the DHR-2 domain of DOCK2 in complex with Rac1 (PDB ID, 2YIN and 3B13) were preprocessed by 'Protein Preparation' in Maestro (Version 9.2; Schrödinger, LLC, New York) and used as a receptor for docking. Generation of the 3D structure of library compounds and ligand preparation were performed by Ligprep program in Maestro. Binding

sites for docking were defined by using the experimentally observed DOCK2-Rac1 interactions (Thr-35, Val-36, Phe-37 and Asp-38 of Rac1) as a reference. Docking calculations were performed using Glide SP mode (Friesner et al., 2004). We applied three additional filters to further screen the hit compounds from each method: extended drug-likeness filter, DOCK2-Rac1 key interactions, and structure alert filter specified by medicinal chemists. Extended drug-likeness filter is based on the Lipinski's rule of five (RO5) for orally absorbed drug (Lipinski et al., 2001, 2004) with some modification: the number of hydrogen-bonding acceptors ≤ 12; the number of hydrogen-bonding donors ≤ 6; molecular weight ≤ 600; AlogP ≤ 6.0. If ligand atoms in the docking pose contact with DOCK2 atoms to form hydrogen bonds (the main chain NH of Val-1539, Met-1540, Gly-1541) or hydrophobic interactions (the side chain C atoms of Phe-1459; only for the hits in SBDD), the atom pairs were judged as forming interaction. To assess the key interactions, simple contact detection program written in MOE SVL Language was employed. The docking poses with one or more hydrogen bonds and one or more hydrophobic interactions were selected for further evaluation. Following the 2D and 3D similarity search, compounds similar to the queries that had TC of greater than 0.95 with MDL Public Key were removed. In addition, compounds with unacceptable structures from the viewpoint of medicinal chemists were also removed. Resulting compounds were clustered by measuring distances by FCFP fingerprint and representative compounds were selected. Pipeline Pilot was used to perform the clustering calculation.

Synthesis of FDOPP, TBOPP, and Their Analogs

General: NMR spectra were recorded on JEOL JNM-ECX500 or JEOL JNM-ECS400 spectrometers. Chemical shifts in $CDCl_3$ were reported in the scale relative to $CHCl_3$ (7.26 ppm for ^1H NMR) and $CDCl_3$, (77.16 ppm for ^{13}C NMR) as an internal reference. Chemical shifts in $(CD_3)_2CO$ were reported in the scale relative to $(CH_3)_2CO$ (2.05 ppm for ^1H NMR) and $(CD_3)_2CO$, (206.26 ppm for ^{13}C NMR) as an internal reference. ESI-mass spectra were measured on JEOL JMS-T100LC AccuTOF spectrometer (for HRMS). Column chromatography was performed with silica gel Merck 60 (230-400 mesh ASTM). Reactions were carried out using flame-dried glassware in dry solvents under an argon atmosphere.

5-(pyrrolidine-1-sulfonyl)-1,2-dihydropyridine-2-one:

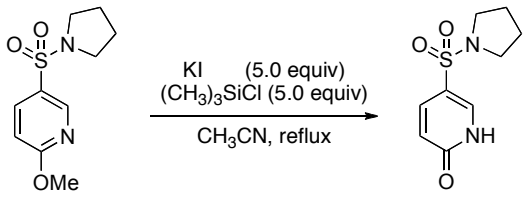

To a solution of 2-methoxy-5-(pyrrolidine-1-sulfonyl)-pyridine (1.4 g, 5.9 mmol) in CH_3CN (120 ml)

were added potassium iodide (4.9 g, 30 mmol) and chlorotrimethylsilane (3.8 ml) at room temperature. The mixture was stirred under reflux for 3 hr, and then 10% $Na_2S_2O_3$ aqueous solution was added. The mixture was extracted with AcOEt (x 3), and the combined organic layers were washed with water and brine. The organic layer was dried over $MgSO_4$ and concentrated under reduced pressure to afford a pale yellow solid in quantitative yield, which was used for the next step without further purification; ^{1}H NMR (500 MHz, Acetone-d_6, 23ºC, δ): 7.99 (d, J = 2.9 Hz, 1H), 7.71 (dd, J = 9.7, 2.9 Hz, 1H), 6.46 (d, J = 9.7 Hz, 1H), 3.15 - 3.29 (m, 4H), 1.74 - 1.89 (m, 4H); ^{13}C NMR (125 MHz, Acetone-d_6, 23ºC, δ): 162.6, 139.9, 138.7, 121.6, 116.5, 48.8, 26.0.

2-bromo-1-(1-(4-fluorobenzyl)-2,5-dimethyl-1*H*-pyrrol-3-yl)ethanone:

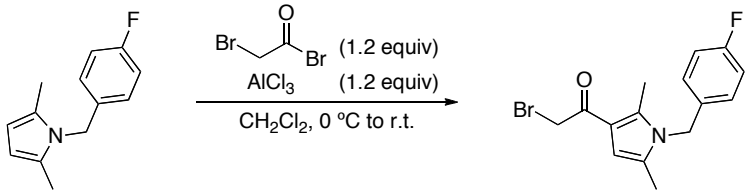

To a flame dried flask with aluminum chloride (480 mg, 3.6 mmol) was added CH_2Cl_2 (45 ml). The mixture was cooled to 0ºC, and then bromoacetylbromide (0.31 ml, 3.6 mmol) was added. The reaction mixture was stirred at 0ºC for 20 min. 4-Fluorobenzyl pyrrole (610 mg, 3.0 mmol) was added and the mixture was stirred at 0ºC for 2 hr. The solution was poured into an ice bath and diluted with CH_2Cl_2. The mixture was extracted with CH_2Cl_2 (x 3), and the combined organic layers were washed with water and brine successively. The organic layer was dried over $MgSO_4$, and concentrated in vacuo. The residue was purified by column chromatography (silica gel, hexane:AcOEt = 5:1) to give a pale brown solid in 35% yield (274 mg, 0.84 mmol); ^{1}H NMR (500 MHz, $CDCl_3$, 23ºC, δ): 7.01 (dd, J = 8.6, 8.6 Hz, 2H), 6.86 (dd, J = 8.6, 5.2 Hz, 2H), 6.31 (s, 1H), 5.02 (s, 2H), 4.23 (s, 2H), 2.49 (s, 3H), 2.13 (s, 3H); ^{13}C NMR (125 MHz, $CDCl_3$, 23ºC, δ): 187.8, 162.6 (d, $J_{(C-F)}$ = 246.5 Hz), 137.9, 132.5 (d, $J_{(C-F)}$ = 3.6 Hz), 128.9, 127.6 (d, $J_{(C-F)}$ = 8.4 Hz), 117.4, 116.4 (d, $J_{(C-F)}$ = 21.6 Hz), 108.5, 46.5, 33.9, 12.6, 12.3; HRMS (ESI-MS) calcd. for $C_{15}H_{15}BrFN\ Na^+O$ [M+Na^+] 346.0219; found 346.0228.

1-(2-(1-(4-fluorobenzyl)-2,5-dimethyl-1*H*-pyrrol-3-yl)-2-oxoethyl)-5-(pyrrolidin-1-ylsulfonyl)pyridin-2(1*H*)-one: (compound 1, FDOPP)

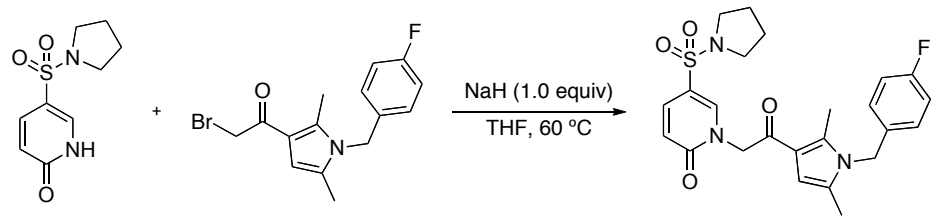

To a solution of 5-(pyrrolidine-1-sulfonyl)-1,2-dihydropyridine-2-one (11.4 mg, 0.05 mmol) in THF (0.4 ml) was added sodium hydride (60% dispersion in mineral oil, 2.0 mg, 0.05 mmol), and the mixture was stirred at 60ºC for 1 hr. A solution of 2-bromo-1-(1-(4-fluorobenzyl)-2,5-dimethyl-1*H*-pyrrol-3-yl)ethanone (16.3 mg, 0.05 mmol) in THF (0.3 ml) was added, and the mixture was further stirred at 60ºC for 5 hr. After cooling down to room temperature, the reaction was quenched by adding water. The mixture was extracted with CH_2Cl_2 (x 3), and the combined organic layers were washed with water and brine successively. The organic layer was dried over $MgSO_4$, and concentrated in vacuo. The residue was purified by column chromatography (silica gel, CH_2Cl_2:AcOEt = 5:1) to give FDOPP as pale yellow solid in 86% yield (20 mg, 0.043 mmol); ^{1}H NMR (500 MHz, $CDCl_3$, 23ºC, δ): 7.89 (d, *J* = 2.6 Hz, 1H), 7.63 (dd, *J* = 9.5, 2.6 Hz, 1H), 6.98 - 7.06 (m, 2H), 6.81 - 6.91 (m, 2H), 6.61 (d, *J* = 9.5 Hz, 1H), 6.38 (s, 1H), 5.19 (s, 2H), 5.03 (s, 2H), 3.21 - 3.37 (m, 4H), 2.45 (s, 3H), 2.15 (s, 3H), 1.83 - 1.96(m, 4H); ^{13}C NMR (125 MHz, $CDCl_3$, 23ºC, δ): 186.4, 162.0 (d, $J_{(C-F)}$ = 246.5 Hz), 161.5, 142.4, 136.8, 136.4, 131.8 (d, $J_{(C-F)}$ = 3.0 Hz), 128.8, 127.0 (d, $J_{(C-F)}$ = 8.4 Hz), 120.3, 116.9, 115.8 (d, $J_{(C-F)}$ = 21.6 Hz), 115.5, 106.8, 54.8, 47.9, 46.0, 25.2, 12.1, 11.7; HRMS (ESI-MS) calcd. for $C_{24}H_{26}FN_3NaO_4S^+$ [M+Na^+] 494.1526; found 494.1503.

1-(2-(1-(4-fluorobenzyl)-2,5-dimethyl-1*H*-pyrrol-3-yl)-2-oxoethyl)pyridin-2(1*H*)- one: (compound 2)

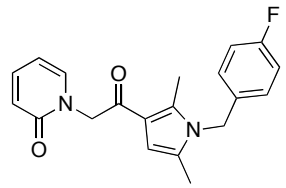

Compound **2** was synthesized from pyridone (37.0 mg, 0.39 mmol) and 2-bromo-1-(1-(4-fluorobenzyl)-2,5-dimethyl-1*H*-pyrrol-3-yl)ethanone (120 mg, 0.37 mmol). By following the synthetic procedure of FDOPP, compound **2** was obtained as pale brown solid in 57% yield (71.2 mg, 0.21 mmol) after purification by column chromatography (silica gel, Hexane:AcOEt = 1:2 to 0:2); ^{1}H NMR (500 MHz, $CDCl_3$, 23ºC, δ): 7.36 (ddd, *J* = 9.1, 7.0, 2.0 Hz, 1H), 7.22 (dd, *J* = 7.0, 2.0 Hz, 1H), 6.98 - 7.05 (m, 2H), 6.85 (dd, *J* = 8.5, 5.5 Hz, 2H), 6.60 (d, *J* = 9.1 Hz, 1H), 6.42 (s, 1H), 6.19 (ddd, *J* = 7.0, 7.0, 1.5 Hz, 1H), 5.16 (s, 2H), 5.01 (s, 2H), 2.46 (s, 3H), 2.14(s, 3H); ^{13}C NMR (125 MHz,

$CDCl_3$, 23ºC, δ): 188.1, 162.7, 162.3 (d, $J_{(C-F)}$ = 246.5 Hz), 139.9, 138.8, 136.9, 132.2 (d, $J_{(C-F)}$ = 3.0 Hz), 128.7, 127.3 (d, $J_{(C-F)}$ = 8.4 Hz), 120.9, 117.5, 116.1 (d, $J_{(C-F)}$ = 21.6 Hz), 107.3, 105.7, 54.9, 46.2, 12.3, 11.9; HRMS (ESI-MS) calcd. for $C_{20}H_{19}FN_2NaO_2^+$ [M+Na^+] 361.1329; found 361.1330.

***N*,*N*-diethyl-6-oxo-1,6-dihydropyridine-3-sulfonamide:**

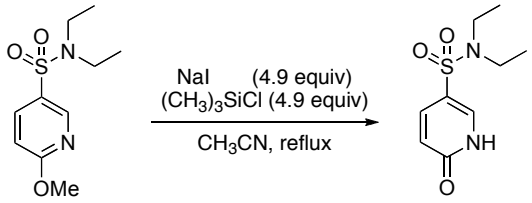

To a solution of *N*,*N*-diethyl-6-methoxypyridine-3-sulfonamide (158 mg, 0.65 mmol) in CH_3CN (8 ml) were added sodium iodide (480 mg, 3.2 mmol) and chlorotrimethylsilane (0.41 ml, 3.2 mmol) at room temperature. The mixture was stirred under reflux for 3 hr, and then 10% $Na_2S_2O_3$ aqueous solution was added. The mixture was extracted with AcOEt (x 3), and the combined organic layers were washed with water and brine. The organic layer was dried over $MgSO_4$ and concentrated under reduced pressure to afford a pale yellow solid in 89% yield (132 mg, 0.57 mmol), which was used for the next step without further purification; ^{1}H NMR (400 MHz, $CDCl_3$, 23ºC, δ): 7.97 (dd, *J* = 2.7, 0.5 Hz, 1H), 7.70 (dd, *J* = 9.7, 2.7 Hz, 1H), 6.63 (dd, *J* = 9.7, 0.5 Hz, 1H), 3.25 (q, *J* = 7.1 Hz, 4H), 1.18 (t, *J* = 7.1 Hz, 6H); ^{13}C NMR (100 MHz, $CDCl_3$, 23ºC, δ): 164.6, 138.5, 137.4, 121.1, 121.1, 42.1, 14.4.

***N*,*N*-diethyl-1-(2-(1-(4-fluorobenzyl)-2,5-dimethyl-1*H*-pyrrol-3-yl)-2-oxoethyl)-6-oxo-1,6-dihydropyridine-3-sulfonamide: (compound 3)**

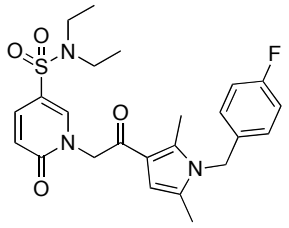

Compound **3** was synthesized from *N*,*N*-diethyl-6-oxo-1,6-dihydropyridine-3-sulfonamide (12.2 mg, 0.053 mmol) and 2-bromo-1-(1-(4-fluorobenzyl)-2,5-dimethyl-1*H*-pyrrol-3-yl)ethanone (17.2 mg, 0.053 mmol). By following the synthetic procedure of FDOPP, compound **3** was obtained as pale brown solid in 25% yield (6.35 mg, 0.013 mmol); ^{1}H NMR (500 MHz, $CDCl_3$, 23ºC, δ): 7.88 (d, *J* = 2.6 Hz, 1H), 7.56 (dd, *J* = 9.7, 2.6 Hz, 1H), 6.99 - 7.05 (m, 2H), 6.84 - 6.89 (m, 2H), 6.61 (d, *J* = 9.7 Hz, 1H), 6.39 (s, 1H), 5.17 (s, 2H), 5.03 (s, 2H), 3.28 (q, *J* = 7.2 Hz, 4H), 2.46 (s, 3H), 2.15 (s, 3H), 1.20 (t, *J* = 7.2 Hz, 6H); ^{13}C NMR (125 MHz, $CDCl_3$, 23ºC, δ): 186.6, 162.3 (d, $J_{(C-F)}$ = 246.5 Hz), 161.8, 142.1, 137.1, 136.3, 132.1

(d, $J_{(C-F)}$ = 3.0 Hz), 129.1, 127.3 (d, $J_{(C-F)}$ = 7.8 Hz), 120.8, 118.7, 117.2, 116.1 (d, $J_{(C-F)}$ = 22.2 Hz), 107.1, 55.2, 46.3, 42.2, 14.4, 12.4, 12.0; HRMS (ESI-MS) calcd. for $C_{24}H_{28}FN_3NaO_4S^+$ [M+Na^+] 496.1683; found 496.1665.

1-(2-oxo-2-(1,2,5-trimethyl-1*H*-pyrrol-3-yl)ethyl)-5-(pyrrolidin-1-ylsulfonyl)pyridin-2(1*H*)-one: (compound 4)

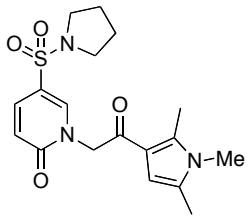

Compound **4** was synthesized from 5-(pyrrolidine-1-sulfonyl)-1,2-dihydropyridine-2-one (22.8 mg, 0.10 mmol) and 2-bromo-1-(1,2,5-trimethyl-1*H*-pyrrol-3-yl)ethanone (22.9 mg, 0.10 mmol). By following the synthetic procedure of FDOPP, compound **4** was obtained as colorless solid in 72% yield (27.1 mg, 0.072 mmol); ^{1}H NMR (400 MHz, $CDCl_3$, 23ºC, δ): 7.88 (d, *J* = 2.5 Hz, 1H), 7.61 (dd, *J* = 9.6, 2.5 Hz, 1H), 6.59 (d, *J* = 9.6 Hz, 1H), 6.29 (s, 1H), 5.13 (s, 2H), 3.41(s, 3H), 3.20 – 3.35 (m, 4H), 2.51 (s, 3H), 2.22 (s, 3H), 1.82 - 1.95(m, 4H); ^{13}C NMR (100 MHz, $CDCl_3$, 23ºC, δ): 186.4, 161.7, 142.7, 137.1, 136.6, 129.0, 120.5, 116.5, 115.6, 106.3, 54.9, 48.2, 30.3, 25.4, 12.5, 12.1; HRMS (ESI-MS) calcd. for $C_{18}H_{23}N_3NaO_4S^+$ [M+Na^+] 400.1307; found 400.1319.

1-(2-oxo-2-phenylethyl)-5-(pyrrolidin-1-ylsulfonyl)pyridin-2(1*H*)-one: (compound 5)

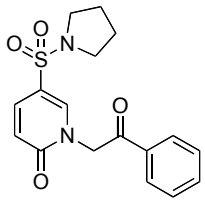

Compound **5** was synthesized from 5-(pyrrolidine-1-sulfonyl)-1,2-dihydropyridine-2-one (75.3 mg, 0.33 mmol) and 2-bromoacetophenone (59.7 mg, 0.30 mmol). By following the synthetic procedure of FDOPP, compound **5** was obtained as colorless solid in 56% yield (57.7 mg, 0.167 mmol) after purification by column chromatography (silica gel, Hexane:AcOEt = 2:1 to 1:2); ^{1}H NMR (400 MHz, $CDCl_3$, 23ºC, δ): 8.00 - 8.04 (m, 2H), 7.89 - 7.93 (m, 1H), 7.62 - 7.69 (m, 2H), 7.49 - 7.58 (m, 2H), 6.62 (d, *J* = 9.6 Hz, 1H), 5.45 (s, 2H), 3.23 - 3.34(m, 4H), 1.84 - 1.95 (m, 4H); ^{13}C NMR (100 MHz, $CDCl_3$, 23ºC, δ): 191.2, 161.3, 141.9, 136.6, 134.3, 134.1, 128.9, 128.0, 120.4, 116.0, 54.0, 47.9, 25.2; HRMS (ESI-MS) calcd. for $C_{17}H_{18}N_2NaO_4S^+$ [M+Na^+] 369.0885; found 369.0893.

1-(2-(biphenyl-4-yl)-2-oxoethyl)-5-(pyrrolidin-1-ylsulfonyl)pyridin-2(1*H*)-one: (compound 6)

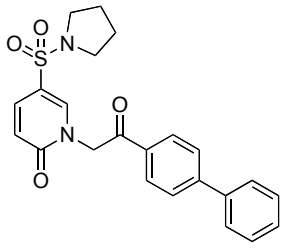

Compound **6** was synthesized from 5-(pyrrolidine-1-sulfonyl)-1,2-dihydropyridine-2-one (34.2 mg, 0.15 mmol) and 1-([1,1'-biphenyl]-4-yl)-2-bromoethanone (41.1 mg, 0.15 mmol). By following the synthetic procedure of FDOPP, compound **6** was obtained as pale yellow solid in 81% yield (51.3mg, 0.12 mmol) after purification by column chromatography (silica gel, Hexane:AcOEt = 1:1); ^{1}H NMR (500 MHz, $CDCl_3$, 23ºC, δ): 8.07(d, *J* = 8.2 Hz, 2H), 7.95 (d, *J* = 2.6 Hz, 1H), 7.74 (d, *J* = 8.2 Hz, 2H), 7.62 - 7.68 (m, 3H), 7.49 (dd, *J* = 7.4, 7.4 Hz, 2H), 7.43 (dd, *J* = 7.4, 7.4 Hz, 1H), 6.63 (d, *J* = 9.8 Hz, 1H), 5.47 (s, 2H), 3.22 - 3.35 (m, 4H), 1.82 - 1.95 (m, 4H); ^{13}C NMR (125 MHz, $CDCl_3$, 23ºC, δ): 191.1, 161.6, 147.2, 142.3, 139.6, 137.0, 136.9, 133.1, 129.2, 128.9, 127.7, 127.4, 120.7, 116.4, 54.3, 48.2, 25.5; HRMS (ESI-MS) calcd. for $C_{23}H_{22}N_2NaO_4S^+$ [M+Na$^+$] 445.1198; found 445.1189.

1-(2-(*p*-terphenyl-4-yl)-2-oxoethyl)-5-(pyrrolidin-1-ylsulfonyl)pyridin-2(1*H*)-one: (compound 7)

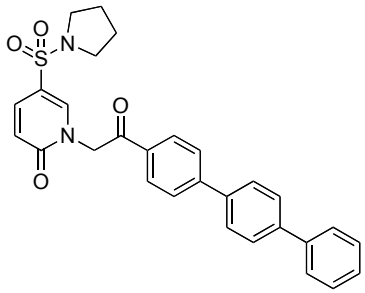

Compound **7** was synthesized from 5-(pyrrolidine-1-sulfonyl)-1,2-dihydropyridine-2-one (22.8 mg, 0.10 mmol) and 1-[1,1':4',1"-terphenyl]-4-yl-2-bromoethanone (38.5 mg, 0.11 mmol). By following the synthetic procedure of FDOPP, compound **7** was obtained as colorless solid in 8% yield (4.1 mg, 0.0082 mmol); ^{1}H NMR (500 MHz, $CDCl_3$, 23ºC, δ): 8.09(d, *J* = 8.3 Hz、2H), 7.94(d, *J* = 2.6 Hz, 1H), 7.80(d, *J* = 8.3 Hz, 2H), 7.73(s, 4H), 7.60 – 7.70(m, 3H), 7.48(dd, *J* = 7.5, 7.5 Hz, 2H), 7.39(dd, *J* = 7.5, 7.5 Hz, 1H), 6.65(d, *J* = 9.8 Hz, 1H), 5.47(s, 2H), 3.22 – 3.37(m, 4H), 1.83 – 1.95(m, 4H);^{13}C NMR (125 MHz, $CDCl_3$, 23ºC, δ): 191.0, 161.6, 146.7, 142.2, 141.6, 140.4, 138.3, 137.0, 137.0, 133.1, 129.1, 129.0, 127.9, 127.8, 127.6, 127.2, 120.7, 116.4, 54.3, 48.2, 25.5; HRMS(ESI-MS) calcd for $C_{29}H_{26}N_2NaO_4S^+$ [M+Na$^+$]

521.1511; found 521.1502.

1-(2-(biphenyl-3-yl)-2-oxoethyl)-5-(pyrrolidin-1-ylsulfonyl)pyridin-2(1*H*)-one: (compound 8)

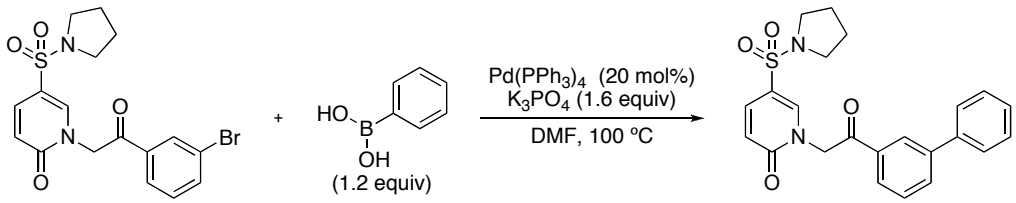

A solution of 1-(2-(3-bromophenyl)-2-oxoethyl)-5-(pyrrolidin-1-ylsulfonyl)pyridin-2(1*H*)-one (28.2 mg, 0.066 mmol), tetrakis(triphenylphosphine)palladium (0.0132 mmol), phenylboronic acid(0.079 mmol) and potassium phosphate (0.11 mmol) in DMF (1.0 ml) was stirred at 100ºC for 48 hr under Ar. After cooling down to room temperature, the reaction mixture was extracted with EtOAc. The organic layer was washed with water and brine successively, dried over $MgSO_4$, and concentrated in vacuo. The residue was purified by column chromatography (silica gel, Hex:AcOEt = 2:3) to afford compound **8** as pale yellow oil in 14% yield (4.0 mg, 0.0095 mmol); ^{1}H NMR (500 MHz, $CDCl_3$, 23ºC, δ): 8.21(t, *J* = 1.7 Hz, 1H), 7.98(ddd, *J* = 7.8, 1.7, 1.1 Hz, 1H), 7.92(d, *J* = 2.6 Hz, 1H), 7.89(ddd, *J* = 7.8, 1.7, 1.1 Hz, 1H), 7.68(dd, *J* = 9.6, 2.6 Hz, 1H), 7.59 – 7.64(m, 3H), 7.46 – 7.52(m, 2H), 7.39 – 7.44(m, 1H), 6.66(d, *J* = 9.6 Hz, 1H), 5.49(s, 2H), 3.27 – 3.35(m, 4H), 1.89 – 1.94(m, 4H); ^{13}C NMR (125 MHz, $CDCl_3$, 23ºC, δ): 191.8, 161.9, 142.8, 142.4, 140.1, 137.3, 135.2, 133.6, 129.9, 129.4, 128.5, 127.6, 127.3, 127.2, 121.1, 116.8, 54.7, 48.5, 25.8; HRMS(ESI-MS) calcd for $C_{23}H_{22}N_2NaO_4S^+$ [M+Na$^+$] 445.1198; found 445.1196.

1-(2-(4'-fluorobiphenyl-4-yl)-2-oxoethyl)-5-(pyrrolidin-1-ylsulfonyl)pyridin-2(1*H*)-one: (compound 9)

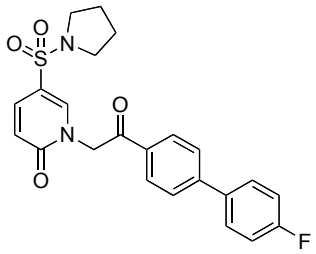

A solution of 1-(2-(4-bromophenyl)-2-oxoethyl)-5-(pyrrolidin-1-ylsulfonyl)pyridin-2(1*H*)-one (17.0 mg, 0.040 mmol), palladium(II) acetate (0.004 mmol) and 1,1'-bis(diphenylphoshino)ferrocene (0.004 mmol) in toluene (1.6 ml) was stirred at 100ºC for 5 min under Ar. To the reaction mixture was added a solution of potassium phosphate (0.16 mmol) in water (0.20 ml), and the mixture was stirred at 100ºC for further 5 min. Then, 4-(fluorophenyl)boronic acid (11.2 mg, 0.08 mmol) was added, and the mixture was further

stirred at 100ºC for 8 hr. After cooling down to room temperature, the reaction mixture was extracted with EtOAc. The organic layer was washed with water and brine successively, dried over $MgSO_4$, and concentrated in vacuo. The residue was purified by column chromatography (silica gel, Hex:AcOEt = 1:2) to afford compound **9** as pale brown solid in 70% yield (12.4 mg, 0.028 mmol); ^{1}H NMR (500 MHz, $CDCl_3$, 23ºC, δ): 8.08(d, *J* = 8.5 Hz, 2H), 7.92(d, *J* = 2.4 Hz, 1H), 7.71(d, *J* = 8.5 Hz, 2H), 7.68(dd, *J* = 9.6, 2.4 Hz, 1H), 7.61(dd, *J* = 8.6, 5.4 Hz, 2H), 7.18(dd, *J* = 8.6, 8.6 Hz, 2H), 6.65(d, *J* = 9.6 Hz, 1H), 5.46(s, 2H), 3.25 – 3.35(m, 4H), 1.86 – 1.96(m, 4H) ; ^{13}C NMR (125 MHz, $CDCl_3$, 23ºC, δ): 191.2, 163.6(d, $J_{(C-F)}$ = 248.9 Hz), 161.9, 146.6, 142.4, 137.3, 136.0(d, $J_{(C-F)}$ = 3.0 Hz), 133.3, 129.4(d, $J_{(C-F)}$ = 8.4 Hz), 129.2, 127.9, 121.0, 116.8, 116.5(d, $J_{(C-F)}$ = 21.6 Hz), 54.5, 48.5, 25.8; HRMS(ESI-MS) calcd for $C_{23}H_{21}N_2NaO_4S^+$ [M+Na^+] 463.1104; found 463.1093.

1-(2-oxo-2-(4'-(trifluoromethyl)biphenyl-4-yl)ethyl)-5-(pyrrolidin-1-ylsulfonyl)pyridin-2(1*H*)-one: (compound 10)

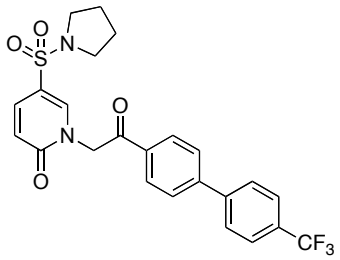

A solution of 1-(2-(4-bromophenyl)-2-oxoethyl)-5-(pyrrolidin-1-ylsulfonyl)pyridin-2(1*H*)-one (17.0 mg, 0.04 mmol), palladium(II) acetate (0.0040 mmol) and 1,1'-bis(diphenylphoshino)ferrocene (0.0040 mmol) in toluene (1.6 ml) was stirred at 100ºC for 5 min under Ar. To the reaction mixture was added a solution of potassium phosphate (0.16 mmol) in degassed water (0.2 ml), and the mixture was stirred at 100ºC for further 5 min. Then, (4-(trifluoromethyl)phenyl)boronic acid (15.2 mg, 0.08 mmol) was added, and the mixture was further stirred at 100ºC for 8 hr. After cooling down to room temperature, the reaction mixture was extracted with EtOAc. The organic layer was washed with water and brine successively, dried over $MgSO_4$, and concentrated in vacuo. The residue was purified by column chromatography (silica gel, CH_2Cl_2:AcOEt = 5:1) to afford compound **10** as pale brown solid in 71% yield (14 mg, 0.029 mmol); ^{1}H NMR (400 MHz, $CDCl_3$, 23ºC, δ): 8.11 (d, *J* = 0.7 Hz, 1H), 8.09 (s, 1H), 7.95 (d, *J* = 2.5 Hz, 1H), 7.72 - 7.76 (m, 6H), 7.61 - 7.69 (m, 1H), 6.63 (d, *J* = 9.6 Hz, 1H), 5.48 (s, 2H), 3.24 - 3.35 (m, 4H), 1.85 - 1.94 (m, 4H); ^{13}C NMR (100 MHz, $CDCl_3$, 23ºC, δ): 191.1, 161.6, 145.6, 143.1, 142.2, 137.0, 133.8, 130.7 (q, $J_{(C-F)}$ = 32.9 Hz), 129.0, 128.0, 127.8, 126.1 (q, $J_{(C-F)}$ = 3.6 Hz), 124.2 (q, $J_{(C-F)}$ = 273.4 Hz), 120.7, 116.5, 54.4, 48.2, 25.5; HRMS (ESI-MS) calcd. for $C_{24}H_{21}F_3N_2NaO_4S^+$ [M+Na^+] 513.1072; found 513.1071.

1-(2-(4'-methoxybiphenyl-4-yl)-2-oxoethyl)-5-(pyrrolidin-1-ylsulfonyl)pyridin-2(1*H*)-one: (compound 11)

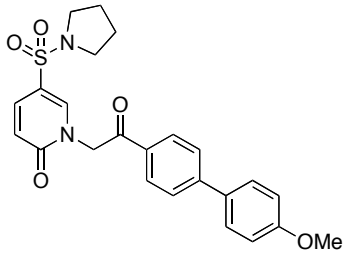

A solution of 1-(2-(4-bromophenyl)-2-oxoethyl)-5-(pyrrolidin-1-ylsulfonyl)pyridin-2(1*H*)-one (17.0 mg, 0.04 mmol), palladium(II) acetate (0.004 mmol) and 1,1'-bis(diphenylphoshino)ferrocene (0.004 mmol) in toluene (1.6 ml) was stirred at 100ºC for 5 min under Ar. To the reaction mixture was added a solution of potassium phosphate (0.16 mmol) in degassed water (0.20 ml), and the mixture was stirred at 100ºC for further 5 min. Then, 4-(methoxyphenyl)boronic acid (12.2 mg, 0.08 mmol) was added, and the mixture was further stirred at 100ºC for 8 hr. After cooling down to room temperature, the reaction mixture was extracted with EtOAc. The organic layer was washed with water and brine successively, dried over $MgSO_4$, and concentrated in vacuo. The residue was purified by column chromatography (silica gel, Hex:AcOEt = 1:2) to afford compound **11** as pale brown solid in 63% yield (11.4 mg, 0.025 mmol);

^{1}H NMR (400 MHz, $CDCl_3$, 23ºC, δ) 8.02 – 8.08(m, 2H), 7.92(d, *J* = 2.6 Hz, 1H), 7.69 – 7.73(m, 2H), 7.67(dd, *J* = 9.6, 2.6 Hz, 1H), 7.57 – 7.63(m, 2H), 6.96 – 7.04(m, 2H), 6.65(d, *J* = 9.6 Hz, 1H), 5.46(s, 2H), 3.88(s, 3H), 3.25 – 3.35(m, 4H), 1.82 – 1.95(m, 4H); ^{13}C NMR (100 MHz, $CDCl_3$, 23ºC, δ): 190.9, 161.6, 160.4, 146.9, 142.2, 137.0, 132.4, 131.9, 128.9, 128.6, 127.1, 120.8, 116.4, 114.7, 55.6, 54.2, 48.3, 25.5; HRMS(ESI-MS) calcd for $C_{24}H_{24}N_2NaO_5S^+$ [M+Na^+] 475.1304; found 475.1288.

1-(2-(2'-fluorobiphenyl-4-yl)-2-oxoethyl)-5-(pyrrolidin-1-ylsulfonyl)pyridin-2(1*H*)-one: (compound 12)

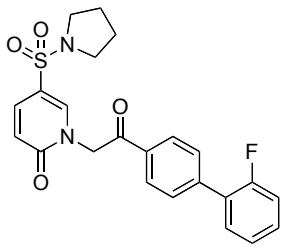

A solution of 1-(2-(4-bromophenyl)-2-oxoethyl)-5-(pyrrolidin-1-ylsulfonyl)pyridin-2(1*H*)-one (21.2 mg,

0.05 mmol), palladium(II) acetate (0.005 mmol) and 1,1'-bis(diphenylphoshino)ferrocene (0.005 mmol) in toluene (3.0 ml) was stirred at 100ºC for 5 min under Ar. To the reaction mixture was added a solution of potassium phosphate (0.20 mmol) in degassed water (0.30 ml), and the mixture was stirred at 100ºC for further 5 min. Then, 2-(fluorophenyl)boronic acid (13.9 mg, 0.10 mmol) was added, and the mixture was further stirred at 100ºC for 8 hr. After cooling down to room temperature, the reaction mixture was extracted with EtOAc. The organic layer was washed with water and brine successively, dried over $MgSO_4$, and concentrated in vacuo. The residue was purified by column chromatography (silica gel, CH_2Cl_2:AcOEt = 5:1) to afford compound **12** as colorless oil in 26% yield (5.7 mg, 0.0129 mmol); ^{1}H NMR (500 MHz, $CDCl_3$, 23ºC, δ): 8.06 – 8.11(m, 2H), 7.93(d, *J* = 2.6 Hz, 1H), 7.73(dd, *J* = 8.4, 1.6 Hz 2H), 7.68(dd, *J* = 9.6, 2.6 Hz, 1H), 7.48(ddd, *J* = 7.8, 7.8, 1.6 Hz, 1H), 7.36 – 7.43(m, 1H), 7.25 - 7.28(m, 1H), 7.17 – 7.23(m, 1H), 6.65(d, *J* = 9.6 Hz, 1H), 5.47(s, 2H), 3.25 – 3.35(m, 4H), 1.85 – 1.95(m, 4H); ^{13}C NMR (125 MHz, $CDCl_3$, 23ºC, δ): 191.4, 161.9, 160.2(d, $J_{(C-F)}$ = 248.9 Hz), 142.5(d, $J_{(C-F)}$ = 1.2 Hz), 142.4, 137.3, 133.6, 131.0(d, $J_{(C-F)}$ = 3.0 Hz), 130.7(d, $J_{(C-F)}$ = 8.4 Hz), 130.1(d, $J_{(C-F)}$ = 3.6 Hz), 128.7, 127.9(d, *J* = 13.2 Hz), 125.1(d, $J_{(C-F)}$ = 3.6 Hz), 121.0, 116.8(d, $J_{(C-F)}$ = 22.2 Hz), 116.8, 54.6, 48.5, 25.8; HRMS(ESI-MS) calcd for $C_{23}H_{21}FN_2NaO_4S^+$ [M+Na^+] 463.1104; found 463.1096.

1-(2-oxo-2-(2'-(trifluoromethyl)biphenyl-4-yl)ethyl)-5-(pyrrolidin-1-ylsulfonyl)pyridin-2(1*H*)-one: (compound 13)

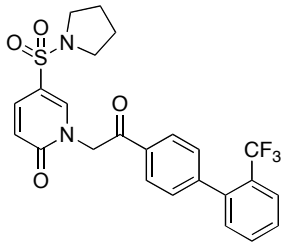

A solution of 1-(2-(4-bromophenyl)-2-oxoethyl)-5-(pyrrolidin-1-ylsulfonyl)pyridin-2(1*H*)-one (21.2 mg, 0.05 mmol), palladium(II) acetate (0.005 mmol) and 1,1'-bis(diphenylphoshino)ferrocene (0.005 mmol) in toluene (3.0 ml) was stirred at 100ºC for 5 min under Ar. To the reaction mixture was added a solution of potassium phosphate (0.20 mmol) in degassed water (0.30 ml), and the mixture was stirred at 100ºC for further 5 min. Then, (2-(trifluoromethyl)phenyl)boronic acid (18.9 mg, 0.10 mmol) was added, and the mixture was further stirred at 100ºC for 8 hr. After cooling down to room temperature, the reaction mixture was extracted with EtOAc. The organic layer was washed with water and brine successively, dried over $MgSO_4$, and concentrated in vacuo. The residue was purified by column chromatography (silica gel, CH_2Cl_2:AcOEt = 5:1) to afford compound **13** as colorless solid in quantitative yield (25.1 mg, 0.05 mmol); ^{1}H NMR (500 MHz, $CDCl_3$, 23ºC, δ): 8.04 – 8.08(m, 2H), 7.93(d, *J* = 2.6 Hz, 1H), 7.79(d, *J*

= 7.8 Hz, 1H), 7.68(dd, *J* = 9.6, 2.6 Hz, 1H), 7.61(dd, *J* = 7.5, 7.5 Hz, 1H), 7.48 – 7.56(m, 3H), 7.33(d, *J* = 7.5 Hz, 1H), 6.66(d, *J* = 9.6 Hz, 1H), 5.48(s, 2H), 3.27 – 3.34(m, 4H), 1.86 – 1.95(m, 4H); ^{13}C NMR (125 MHz, $CDCl_3$, 23ºC, δ): 191.2, 161.6, 146.3, 142.1, 139.8(q, $J_{(C-F)}$ = 1.8 Hz), 137.1, 133.6, 131.7, 131.6, 129.9(q, $J_{(C-F)}$ = 1.6 Hz), 128.5(q, $J_{(C-F)}$ = 30.4 Hz), 128.4, 127.9, 126.5(q, $J_{(C-F)}$ = 5.2 Hz), 124.1(q, $J_{(C-F)}$ = 273.7 Hz), 120.8, 116.6, 54.4, 48.2, 25.5; HRMS(ESI-MS) calcd for $C_{24}H_{21}F_3N_2NaO_4S^+$ [M+Na^+] 513.1072; found 513.1049.

1-(2-(2'-methoxybiphenyl-4-yl)-2-oxoethyl)-5-(pyrrolidin-1-ylsulfonyl)pyridin-2(1*H*)-one: (compound 14)

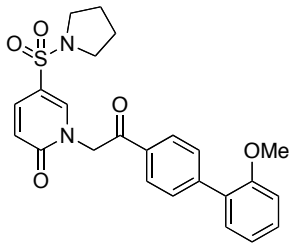

A solution of 1-(2-(4-bromophenyl)-2-oxoethyl)-5-(pyrrolidin-1-ylsulfonyl)pyridin-2(1*H*)-one (21.2 mg, 0.05 mmol), palladium(II) acetate (0.005 mmol) and 1,1'-bis(diphenylphoshino)ferrocene (0.005 mmol) in toluene (3.0 ml) was stirred at 100ºC for 5 min under Ar. To the reaction mixture was added a solution of potassium phosphate (0.20 mmol) in degassed water (0.30 ml), and the mixture was stirred at 100ºC for further 5 min. Then, 2-(methoxyphenyl)boronic acid (15.2 mg, 0.10 mmol) was added, and the mixture was further stirred at 100ºC for 8 hr. After cooling down to room temperature, the reaction mixture was extracted with EtOAc. The organic layer was washed with water and brine successively, dried over $MgSO_4$, and concentrated in vacuo. The residue was purified by column chromatography (silica gel, CH_2Cl_2:AcOEt = 5:1) to afford compound **14** as pale yellow solid in 94% yield (21.2 mg, 0.047 mmol); ^{1}H NMR (500 MHz, $CDCl_3$, 23ºC, δ): 8.04(d, *J* = 8.6 Hz, 2H), 7.92(d, *J* = 2.6 Hz, 1H), 7.60 – 7.75(m, 3H), 7.30 – 7.40(m, 2H), 7.03 – 7.09(m, 1H), 7.02(d, *J* = 8.4 Hz, 1H), 6.64(d, *J* = 9.5 Hz, 1H), 5.46(s, 2H), 3.83(s, 3H), 3.25 – 3.35(m, 4H), 1.85 – 1.93(m, 4H); ^{13}C NMR (125 MHz, $CDCl_3$, 23ºC, δ): 191.2, 161.6, 156.6, 145.3, 142.2, 137.0, 132.7, 130.8, 130.3, 130.0, 129.2, 128.0, 121.2, 120.7, 116.4, 111.6, 55.7, 54.3, 48.2, 25.5; HRMS(ESI-MS) calcd for $C_{24}H_{24}N_2NaO_5S^+$ [M+Na^+] 475.1304; found 475.1281.

1-(2-(3'-fluorobiphenyl-4-yl)-2-oxoethyl)-5-(pyrrolidin-1-ylsulfonyl)pyridin-2(1*H*)-one: (compound 15)

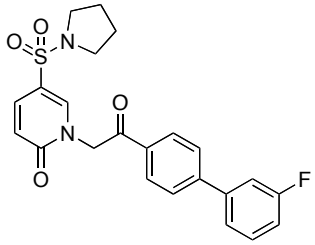

A solution of 1-(2-(4-bromophenyl)-2-oxoethyl)-5-(pyrrolidin-1-ylsulfonyl)pyridin-2(1*H*)-one (21.2 mg, 0.05 mmol), palladium(II) acetate (0.005 mmol) and 1,1'-bis(diphenylphoshino)ferrocene (0.005 mmol) in toluene (3.0 ml) was stirred at 100ºC for 5 min under Ar. To the reaction mixture was added a solution of potassium phosphate (0.20 mmol) in degassed water (0.30 ml), and the mixture was stirred at 100ºC for further 5 min. Then, 3-(fluorophenyl)boronic acid (13.9 mg, 0.10 mmol) was added, and the mixture was further stirred at 100ºC for 8 hr. After cooling down to room temperature, the reaction mixture was extracted with EtOAc. The organic layer was washed with water and brine successively, dried over $MgSO_4$, and concentrated in vacuo. The residue was purified by column chromatography (silica gel, CH_2Cl_2:AcOEt = 5:1) to afford compound **15** as pale brown solid in 97% yield (21.3 mg, 0.0484 mmol); ^{1}H NMR (400 MHz, $CDCl_3$, 23ºC, δ): 8.09(d, *J* = 8.3 Hz, 2H), 7.93(d, *J* = 2.7 Hz, 1H), 7.74(d, *J* = 8.3 Hz, 2H), 7.68(dd, *J* = 9.6, 2.7 Hz, 1H), 7.40 – 7.50(m, 2H), 7.30 – 7.40(m, 1H), 7.10 – 7.15(m, 1H), 6.66(d, *J* = 9.6 Hz, 1H), 5.46(s, 2H), 3.25 – 3.35(m, 4H), 1.85 – 1.95(m, 4H); ^{13}C NMR (125 MHz, $CDCl_3$, 23ºC, δ):191.3, 163.6(d, $J_{(C-F)}$ = 246.5 Hz), 161.9, 146.2(d, $J_{(C-F)}$ = 2.4 Hz), 142.4, 142.1(d, $J_{(C-F)}$ = 7.8 Hz), 137.3, 133.8, 131.0(d, $J_{(C-F)}$ = 8.4 Hz), 129.3, 128.1, 123.4(d, $J_{(C-F)}$ = 3.0 Hz), 121.0, 116.8, 115.9(d, $J_{(C-F)}$ = 21.0 Hz), 114.7(d, $J_{(C-F)}$ = 22.2 Hz), 54.6, 48.5, 25.8; HRMS(ESI-MS) calcd for $C_{23}H_{21}FN_2NaO_4S^+$ [M+Na^+] 463.1104; found 475.1096.

1-(2-(3'-(trifluoromethyl)-[1,1'-biphenyl]-4-yl)-2-oxoethyl)-5-pyrrolidinylsulfonyl-2(1*H*)-pyridone: (compound 16, TBOPP)

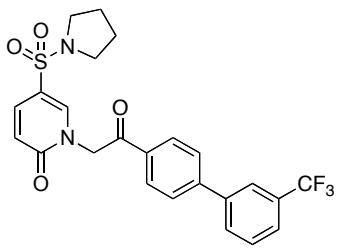

A solution of 1-(2-(4-bromophenyl)-2-oxoethyl)-5-(pyrrolidin-1-ylsulfonyl)pyridin-2(1*H*)-one (21.2 mg, 0.050 mmol), palladium(II) acetate (0.0050 mmol) and 1,1'-bis(diphenylphoshino)ferrocene (0.0050 mmol) in toluene (3.0 ml) was stirred at 100ºC for 5 min under Ar. To the reaction mixture was added a

solution of potassium phosphate (0.20 mmol) in degassed water (0.30 ml), and the mixture was stirred at 100ºC for further 5 min. Then, (3-(trifluoromethyl)phenyl)boronic acid (19.0 mg, 0.10 mmol) was added, and the mixture was further stirred at 100ºC for 8 hr. After cooling down to room temperature, the reaction mixture was extracted with EtOAc. The organic layer was washed with water and brine successively, dried over $MgSO_4$, and concentrated in vacuo. The residue was purified by column chromatography (silica gel, CH_2Cl_2:AcOEt = 5:1) to afford compound **16** as yellow oil in 92% yield (22.6 mg, 0.046 mmol); ^{1}H NMR (500 MHz, $CDCl_3$, 23ºC, δ): 8.09-8.14 (m, 2H), 7.93 (d, *J* = 2.6 Hz, 1H), 7.88 (s, 1H), 7.82 (d, *J* = 7.7 Hz, 1H), 7.74 - 7.79 (m, 2H), 7.69 (d, *J* = 7.7 Hz, 1H), 7.68 (dd, *J* = 9.6, 2.6 Hz, 1H), 7.62 (dd, *J* = 7.7, 7.7 Hz, 1H), 6.66 (d, *J* = 9.6 Hz, 1H), 5.47 (s, 2H), 3.29 - 3.34 (m, 4H), 1.88 - 1.94 (m, 4H); ^{13}C NMR (125 MHz, $CDCl_3$, 23ºC, δ): 191.1, 161.6, 145.5, 142.2, 140.4, 137.0, 133.7, 131.6 (q, $J_{(C-F)}$ = 32.4 Hz), 130.7, 129.7, 129.0, 127.8, 125.3(q, $J_{(C-F)}$ = 3.6 Hz) 124.2 (q, $J_{(C-F)}$ = 3.6 Hz), 124.1 (q, $J_{(C-F)}$ = 272.3 Hz), 120.7, 116.4, 54.4, 48.2, 25.5; HRMS (ESI-MS) calcd. for $C_{24}H_{21}F_3N_2NaO_4S^+$ [M+Na^+] 513.1072; found 513.1078.

1-(2-(3'-methoxybiphenyl-4-yl)-2-oxoethyl)-5-(pyrrolidin-1-ylsulfonyl)pyridin-2(1*H*)-one: (compound 17)

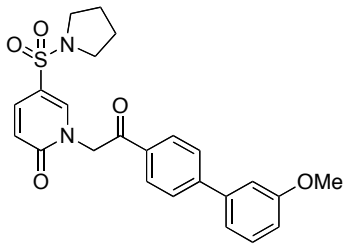

A solution of 1-(2-(4-bromophenyl)-2-oxoethyl)-5-(pyrrolidin-1-ylsulfonyl)pyridin-2(1*H*)-one (21.2 mg, 0.05 mmol), palladium(II) acetate (0.005 mmol) and 1,1'-bis(diphenylphoshino)ferrocene (0.005 mmol) in toluene (3.0 ml) was stirred at 100ºC for 5 min under Ar. To the reaction mixture was added a solution of potassium phosphate (0.20 mmol) in degassed water (0.30 ml), and the mixture was stirred at 100ºC for further 5 min. Then, 3-(methoxyphenyl)boronic acid (15.2 mg, 0.10 mmol) was added, and the mixture was further stirred at 100ºC for 8 hr. After cooling down to room temperature, the reaction mixture was extracted with EtOAc. The organic layer was washed with water and brine successively, dried over $MgSO_4$, and concentrated in vacuo. The residue was purified by column chromatography (silica gel, CH_2Cl_2:AcOEt = 5:1) to afford compound **17** as colorless oil in 79% yield (17.9 mg, 0.0396 mmol); ^{1}H NMR (500 MHz, $CDCl_3$, 23ºC, δ): 8.05 – 8.08(m, 2H), 7.93(d, *J* = 2.4 Hz, 1H), 7.73 – 7.90(m, 2H), 7.67(dd, *J* = 9.9, 2.4 Hz, 1H), 7.41(dd. *J* = 8.0, 8.0 Hz, 1H), 7.23(ddd, *J* = 8.0, 2.1, 0.8 Hz, 1H), 7.16(dd, *J* = 2.1, 2.1 Hz, 1H), 6.97(ddd, *J* = 8.0, 2.1, 0.8 Hz, 1H), 6.65(d, *J* = 9.9 Hz, 1H), 5.46(s, 2H),

3.89(s, 3H), 3.26 – 3.34(m, 4H), 1.88 – 1.94(m, 4H); ^{13}C NMR (125 MHz, $CDCl_3$, 23ºC, δ): 190.8, 161.4, 160.0, 146.9, 141.9, 140.8, 136.7, 132.9, 130.0, 128.6, 127.6, 120.5, 119.7, 116.2, 113.8, 113.0, 55.3, 54.1, 48.0, 25.3; HRMS(ESI-MS) calcd for $C_{24}H_{24}N_2NaO_5S^+$ [M+Na^+] 475.1304; found 475.1282.

1-(2-(3'-chlorobiphenyl-4-yl)-2-oxoethyl)-5-(pyrrolidin-1-ylsulfonyl)pyridin-2(1*H*)-one: (compound 18)

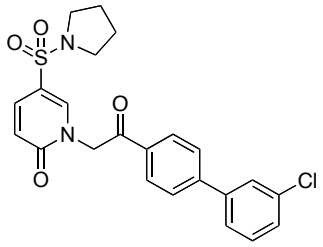

A solution of 1-(2-(4-bromophenyl)-2-oxoethyl)-5-(pyrrolidin-1-ylsulfonyl)pyridin-2(1*H*)-one (21.2 mg, 0.05 mmol), palladium(II) acetate (0.005 mmol) and 1,1'-bis(diphenylphoshino)ferrocene (0.005 mmol) in toluene (3.0 ml) was stirred at 100ºC for 5 min under Ar. To the reaction mixture was added a solution of potassium phosphate (0.20 mmol) in degassed water (0.30 ml), and the mixture was stirred at 100ºC for further 5 min. Then, 3-(chlorophenyl)boronic acid (15.6 mg, 0.10 mmol) was added, and the mixture was further stirred at 100ºC for 8 hr. After cooling down to room temperature, the reaction mixture was extracted with EtOAc. The organic layer was washed with water and brine successively, dried over $MgSO_4$, and concentrated in vacuo. The residue was purified by column chromatography (silica gel, CH_2Cl_2:AcOEt = 5:1) to afford compound **18** as pale brown oil in 77 % yield (17.6 mg, 0.0385 mmol); ^{1}H NMR (500 MHz, $CDCl_3$, 23ºC, δ) : 8.09(d, *J* = 8.0 Hz, 2H), 7.92(d, *J* = 2.0 Hz, 1H), 7.73(d, *J* = 8.0 Hz, 2H), 7.66 - 7.71(m, 1H), 7.63(d, *J* = 0.9 Hz, 1H), 7.50 – 7.56(m, 1H), 7.38 – 7.46(m, 2H), 6.66(d, *J* = 9.8 Hz, 1H), 5.46(s, 2H), 3.25 - 3.40(m, 4H), 1.85 – 2.00(m, 4H); ^{13}C NMR (125 MHz, $CDCl_3$, 23ºC, δ): 191.0, 161.6, 145.9, 142.1, 141.4, 137.1, 135.2, 133.6, 130.5, 129.0, 128.8, 127.9, 127.6, 125.6, 120.8, 116.6, 54.3, 48.3, 25.6; HRMS(ESI-MS) calcd for $C_{23}H_{21}ClN_2NaO_4S^+$ [M+Na^+] 479.0809; found 479.0814.

1-(2-(4-(naphthalen-2-yl)phenyl)-2-oxoethyl)-5-(pyrrolidin-1-ylsulfonyl)pyridin-2(1*H*)-one: (compound 19)

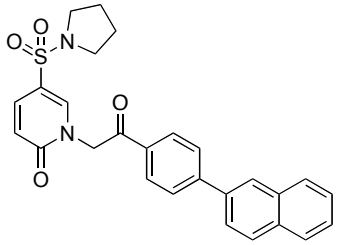

A solution of 1-(2-(4-bromophenyl)-2-oxoethyl)-5-(pyrrolidin-1-ylsulfonyl)pyridin-2(1*H*)-one (10.7 mg, 0.025 mmol), palladium(II) acetate (0.003 mmol) and 1,1'-bis(diphenylphoshino)ferrocene (0.003 mmol) in toluene (1.6 ml) was stirred at 100ºC for 5 min under Ar. To the reaction mixture was added a solution of potassium phosphate (1.0 mmol) in degassed water (0.20 ml), and the mixture was stirred at 100ºC for further 5 min. Then, 2-(naphthalenyl)boronic acid (8.6 mg, 0.05 mmol) was added, and the mixture was further stirred at 100ºC for 8 hr. After cooling down to room temperature, the reaction mixture was extracted with EtOAc. The organic layer was washed with water and brine successively, dried over $MgSO_4$, and concentrated in vacuo. The residue was purified by column chromatography (silica gel, CH_2Cl_2:AcOEt = 5:1) to afford compound **19** as yellow oil in 69% yield (8.1 mg, 0.017 mmol); ^{1}H NMR (500 MHz, $CDCl_3$, 23ºC, δ): 8.13(s, 1H), 8.12(s, 2H), 7.84 – 8.00(m, 6H), 7.65(m, 2H), 7.50 – 7.58(m, 2H), 6.66(d, *J* = 9.7 Hz, 1H), 5.49(s, 2H), 3.26 – 3.36(m, 4H), 1.86 – 1.96(m, 4H); ^{13}C NMR (125 MHz, $CDCl_3$, 23ºC, δ): 191.3, 161.9, 147.5, 142.5, 137.3, 137.1, 133.9, 133.6, 133.3, 129.3, 129.2, 128.8, 128.3, 128.1, 127.1, 127.1, 127.0, 125.4, 121.0, 116.8, 54.6, 48.5, 25.8; HRMS(ESI-MS) calcd for $C_{27}H_{24}N_2NaO_4S^+$ [M+Na^+] 495.1355; found 495.1339.

1-(2-(*m*-terphenyl-4-yl)-2-oxoethyl)-5-(pyrrolidin-1-ylsulfonyl)pyridin-2(1*H*)-one:

(compound 20)

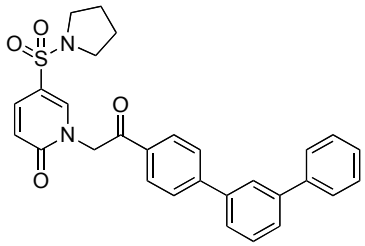

A solution of 1-(2-(4-bromophenyl)-2-oxoethyl)-5-(pyrrolidin-1-ylsulfonyl)pyridin-2(1*H*)-one (21.2 mg, 0.05 mmol), palladium(II) acetate (0.005 mmol) and 1,1'-bis(diphenylphoshino)ferrocene (0.005 mmol) in toluene (3.0 ml) was stirred at 100ºC for 5 min under Ar. To the reaction mixture was added a solution of potassium phosphate (0.2 mmol) in degassed water (0.3 ml), and the mixture was stirred at 100ºC for further 5 min. Then, (biphenyl-3-yl)boronic acid (19.8 mg, 0.1 mmol) was added, and the mixture was further stirred at 100ºC for 8 hr. After cooling down to room temperature, the reaction mixture was

extracted with EtOAc. The organic layer was washed with water and brine successively, dried over $MgSO_4$, and concentrated in vacuo. The residue was purified by column chromatography (silica gel, CH_2Cl_2:AcOEt = 5:1) to afford compound **20** as colorless solid in 95% yield (23.8 mg, 0.0477 mmol); ^{1}H NMR (500 MHz, $CDCl_3$, 23ºC, δ): 8.10(d, *J* = 8.4 Hz、2H), 7.94(d, *J* = 2.6 Hz, 1H), 7.83 – 7.85(m, 1H), 7.80(d, *J* = 8.4 Hz, 2H), 7.60 – 7.70(m, 5H), 7.56(dd, *J* = 7.7, 7.7 Hz, 1H), 7.56(dd, *J* = 7.5, 7.5 Hz 2H), 7.40(dd, *J* = 7.5, 7.5 Hz, 1H), 6.65(d, *J* = 9.8 Hz, 1H), 5.48(s, 2H), 3.28 – 3.34(m, 4H), 1.86 – 1.94(m, 4H); ^{13}C NMR (125 MHz, $CDCl_3$, 23ºC, δ): 191.1, 161.6, 147.2, 142.3, 142.2, 140.9, 140.1, 137.0, 133.2, 129.6, 129.0, 128.9, 127.9, 127.8, 127.6, 127.4, 126.4, 126.3, 120.7, 116.4, 54.3, 48.2, 25.5; HRMS(ESI-MS) calcd for $C_{29}H_{26}N_2NaO_4S^+$ [M+Na$^+$] 521.1511; found 521.1499.

1-(2-(4'-chloro-3'-(trifluoromethyl)biphenyl-4-yl)-2-oxoethyl)-5-(pyrrolidin-1-ylsulfonyl)pyridin-2(1*H*)-one: (compound 21)

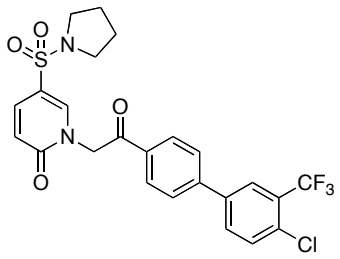

A solution of 1-(2-(4-bromophenyl)-2-oxoethyl)-5-(pyrrolidin-1-ylsulfonyl)pyridin-2(1*H*)-one (21.2 mg, 0.05 mmol), palladium(II) acetate (0.005 mmol) and 1,1'-bis(diphenylphoshino)ferrocene (0.005 mmol) in toluene (3.0 ml) was stirred at 100ºC for 5 min under Ar. To the reaction mixture was added a solution of potassium phosphate (0.2 mmol) in degassed water (0.6 ml), and the mixture was stirred at 100ºC for further 5 min. Then, 4-chloro-3-(trifluoromethyl)phenylboronic acid (67.3 mg, 0.3 mmol) was added, and the mixture was further stirred at 100ºC for 8 hr. After cooling down to room temperature, the reaction mixture was extracted with EtOAc. The organic layer was washed with water and brine successively, dried over $MgSO_4$, and concentrated in vacuo. The residue was purified by column chromatography (silica gel, CH_2Cl_2:AcOEt = 5:1) to afford compound **21** as pale yellow solid in 88% yield (23.0 mg, 0.0438 mmol); ^{1}H NMR (500 MHz, $CDCl_3$, 23ºC, δ): 8.11(d, *J* = 8.3 Hz, 2H), 7.94(d, *J* = 2.6 Hz, 1H), 7.93(s, 1H), 7.70 – 7.75(m, 3H), 7.67(dd, *J* = 9.8, 2.6 Hz, 1H), 7.63(d, *J* = 8.3 Hz, 1H), 6.64(d, *J* = 9.8 Hz, 1H), 5.47(s, 2H), 3.24 – 3.32(m, 4H), 1.81 – 1.92(m, 4H); ^{13}C NMR (125 MHz, $CDCl_3$, 23ºC, δ): 191.0, 161.6, 144.5, 142.1, 138.5, 137.0, 133.9, 132.8(q, $J_{(C-F)}$ = 1.6 Hz), 132.4, 131.5, 129.3(q, $J_{(C-F)}$ = 31.6 Hz), 129.2, 127.8, 126.5(q, $J_{(C-F)}$ = 5.4 Hz), 122.8(q, $J_{(C-F)}$ = 273.1 Hz), 120.8, 116.6, 54.4, 48.2, 25.5; HRMS(ESI-MS) calcd for $C_{24}H_{20}ClF_3N_2NaO_4S^+$ [M+Na$^+$] 547.0682; found 547.0673.

1-(2-(3',5'-bis(trifluoromethyl)biphenyl-4-yl)-2-oxoethyl)-5-(pyrrolidin-1-ylsulfonyl)pyridin-2(1*H*)-one: (compound 22)

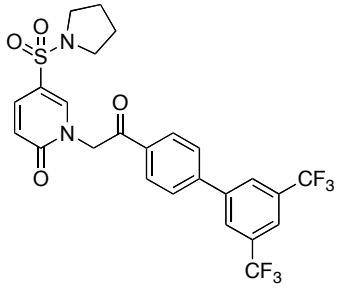

A solution of 1-(2-(4-bromophenyl)-2-oxoethyl)-5-(pyrrolidin-1-ylsulfonyl)pyridin-2(1*H*)-one (42.5 mg, 0.10 mmol), palladium(II) acetate (0.010 mmol) and 1,1'-bis(diphenylphoshino)ferrocene (0.01 mmol) in toluene (1.5 ml) was stirred at 100ºC for 5 min under Ar. To the reaction mixture was added a solution of potassium phosphate (0.4 mmol) in degassed water (0.15 ml), and the mixture was stirred at 100ºC for further 5 min. Then, (3,5-bis(trifluoromethyl)phenyl)boronic acid (51.7 mg, 0.2 mmol) was added, and the mixture was further stirred at 100ºC for 8 hr. After cooling down to room temperature, the reaction mixture was extracted with EtOAc. The organic layer was washed with water and brine successively, dried over $MgSO_4$, and concentrated in vacuo. The residue was purified by column chromatography (silica gel, CH_2Cl_2:AcOEt = 10:1) to afford compound **22** as pale yellow solid in 94% yield (52.7 mg, 0.093 mmol); ^{1}H NMR (500 MHz, $CDCl_3$, 23ºC, δ): 8.14(d, J = 8.3 Hz, 2H), 8.06(s, 2H), 7.97(d, J = 2.6 Hz, 1H), 7.93(s, 1H), 7.76(d, J = 8.3 Hz, 2H), 7.66(dd, J = 9.7, 2.6 Hz, 1H), 6.63(d, J = 9.7 Hz, 1H), 5.49(s, 2H), 3.20 – 3.33(m, 4H), 1.82 – 1.93(m, 4H); ^{13}C NMR (125 MHz, $CDCl_3$, 23ºC, δ): 191.0, 161.6, 143.9, 142.2, 141.8, 137.0, 134.4, 132.7(q, $J_{(C-F)}$ = 33.4 Hz), 129.3, 128.0, 127.5(q, $J_{(C-F)}$ = 3.0 Hz), 123.3(q, $J_{(C-F)}$ = 272.7 Hz), 122.2(q, $J_{(C-F)}$ = 3.6 Hz), 120.7, 116.6, 54.5, 48.2, 25.5; HRMS(ESI-MS) calcd for $C_{25}H_{20}F_6N_2NaO_4S^+$ [M+Na^+] 581.0946; found 581.0942.

In Vitro GEF Assays

Recombinant His-SUMO-tagged DOCK1 DHR-2, DOCK2 DHR-2, Tiam1 DH-PH, and Trio DH-PH proteins were expressed in the Arctic BL21 (DE3) bacterial strain, and purified by Ni-NTA affinity chromatography (Qiagen). The T1500V and N1540K mutations were introduced to the pET28a vector encoding His-SUMO-tagged DOCK1 DHR-2 by PCR mutagenesis with the following primers: T1500V-F: 5'-GAGACAATGCAGTTGGTCAATGACAAGATCAGC-3', T1500V-R: 5'-GCTGAT CTTGTCATTGACCAACTGCATTGTCTC-3', N1540K-F: 5'-ATGGGTGGTTTTGCCAAGTATG AGAAGGCTTTC-3', and N1540K-R: 5'-GAAAGCCTTCTCATACTTGGCAAAACCACCCAT-3'. GST-Rac1 was expressed in BL21 (DE3) bacterial strain and purified by glutathione Sepharose 4B

chromatography (GE HealthCare). The assays consisted of GST-Rac1 (10 μM), Bodipy-FL GTP (2.4 μM; Invitrogen G12411) and GEF proteins (0.05 μM for DOCK1; 0.1 μM for DOCK2 and DOCK5; 1 μM for Trio; 2 μM for Tiam1 depending on the strength of each GEF activity) in the reaction buffer (20 mM MES-NaOH, 150 mM NaCl, 10 mM $MgCl_2$, 20 μM GDP, pH 7.0). GST-Rac1 was loaded with GDP by incubating with the reaction buffer on ice for 30 min, and then mixed with Bodipy-FL GTP (3.6 μM), and allowed to equilibrate at 30°C for 3 min. Recombinant GEF proteins were incubated with compounds or vehicle alone (final concentration of DMSO; 1%) at the indicated concentrations in the reaction buffer for 20 min at room temperature. The reaction was initiated by mixing GDP-loaded Rac1/Bodipy-FL GTP (100 μl) and GEF protein (50 μl) in a final volume of 150 μl and incubating at 30°C. The change in Bodipy-FL-GTP fluorescence (Excitation: 488 nm, Emission: 514 nm) was monitored for 20 min using a Perkin Elmer EnSpire multimode plate reader. Data were fitted using a curve fitting function of the GraphPad Prism 5 program (GraphPad Software), and the initial slope during the first 10 seconds was calculated (RFU/s: relative fluorescent unit per second), and used for comparison of the GEF activity. IC_{50} values were determined by plotting the GEF activity (% of control) over the log concentration of each compound, and fitting with the 'log [inhibitor concentration] vs. response with variable slope model' of Prism 5.

Plasmids and Transfection

H-RasV12 mutant was generated by site-directed mutagenesis. The retroviral vector pMX-IRES-GFP was used to generate the plasmid pMX-H-RasV12-IRES-GFP and pMX-H-Ras WT-IRES-GFP, which were transfected into Platinum-E packaging cells using FuGENE 6 transfection reagent (Promega). The cell culture supernatants were harvested 48 hr after transfection, supplemented with 5 μg/ml polybrene, and used to infect MEFs. The pBJ vector encoding neomycin (pBJ-neo) was used to express the C-terminally FLAG-tagged DOCK1 (pBJ-DOCK1). The expression vector encoding DOCK1 mutant (V1534A) was generated by site-directed mutagenesis. These pBJ vectors were transfected into *Dock1*$^{-/-}$ MEFs with polyethylenimine, and cells were selected with 500 μg/ml G418 (Calbiochem) to develop stable clones. For knock down of mouse DOCK1 by shRNA, the following target sequence was used: 5'-GCACACGAAGTTGCTTCTAAA-3'. The sense and antisense oligonucleotides were annealed and cloned into the pSuper/puro vector (Oligoengine) encoding puromycin, and the resulting plasmid was transfected into 3LL cells with polyethylenimine. Cells were then selected with 1 μg/ml puromycin to develop stable clones. As a control, shRNA targeting irrelevant *lacZ* sequence was also used.

DOCK1 deficient HT1080 and DLD-1 cells were generated by the CRISPR/CAS9 system in

combination with gene targeting by homologous recombination (HR). Two guide sequences within the exon 1 of human *DOCK1* were selected using the CHOPCHOP web tool (https://chopchop.rc.fas.harvard.edu/). For each target, two complementary oligonucleotides (Target 1: 5'-CACCGTACTTCTCCTCGCGCTTGG-3' and 5'-AAACCCAAGCGCGAGGAGAAGTAC-3'; Target 2: 5'-CACCGCGCGAGGAGAAGTACGGCG-3' and 5'-AAACCGCCGTACTTCTCCTCGCGC-3') containing the guide sequence and *Bbs* I ligation adapters were synthesized, annealed and ligated into the *Bbs* I-digested pX330 vector to generate the single guide RNA (sgRNA) vector. To construct the HR targeting vector for each target, the 5' and 3' homology arms (840 and 771 bp for target 1; 983 and 837 bp for target 2) were amplified from the genomic DNA isolated from HT1080 cells by PCR with the following primers:

Target 1/5'-arm_F: 5'-TTCGAATTCTTTCTGCGGCTGCTTCCTCTTGG-3',

Target 1/5'-arm_R: 5'-TCTAGATCTTGGTGGGCACCCAGCGCGTC-3',

Target 1/3'-arm_F: 5'-TCCGGATCCTGGGTGAGCAGCGCCGCCGCC-3',

Target 1/3'-arm_R: 5'-GACGTCGACATTCAGCCGCAAGGGAAAGCCTC-3',

Target 2/5'-arm_F: 5'-TTCGAATTCAAGGATGTCTGTGGATGGTGGGACG-3',

Target 2/5'-arm_R: 5'-TCTAGATCTGGCGTGGGTGAGCAGCGCCGC-3',

Target 2/3'-arm_F: 5'-TCCGGATCCTGGGCACCCAGCGCGTCATGGC-3', and

Target 2/3'-arm_R: 5'-GACGTCGACGTTTCTGCGGCTGCTTCCTCTTG-3'.

The amplified DNAs were inserted into the *EcoR* I-*Bgl* II and *BamH* I-*Sal* I sites of the HR410PA-1 targeting vector (System Biosciences), which carries the GFP expression cassette and puromycin resistance gene between the homology arms. HT1080 and DLD-1 cells were transfected with 1.25 μg of sgRNA vector and 1.25 μg HR targeting vector using 10 μl of Lipofectamine 2000 (Invitrogen) in 6-well plates. 48 hr after transfection, cells were selected in the presence of puromycin (0.8 μg /ml) and cloned by limiting dilution. From the GFP positive and puromycin-resistance cells, DOCK1-deficient clones were identified by examining DOCK1 expression by immunoblotting. Homologous recombination was verified by PCR on genomic DNA.

TIAM1 deficient DLD-1 cells were also generated with the CRISPR/CAS9 system by using a guide sequence within the exon 5 of human TIAM1. For this purpose, two complementary oligonucleotides (5'-CACCGCAGAGCATGCCAGACACTG-3' and 5'-AAACCAGTGTCTGGCA TGCTCTGC-3') containing the guide sequence and *Bbs* I ligation adapters were synthesized, annealed and ligated into the *Bbs* I-digested pX330 vector to generate the sgRNA vector. To construct the HR targeting vector, the 5' and 3' homology arms (896 and 713 bp) were amplified from the genomic DNA isolated from DLD-1 cells by PCR with the following primers:

5'-arm_F: 5'- TCTGAATTCACCCATTGTCAGGGAGGGAAGGAG-3',

5'-arm_R: 5'- TTCAGATCTACAGAGGCTGCTGTGAGGACGATG-3',

3'-arm_F: 5'- TCCGGATCCAGGAGAGCAGGCTTTACGGGGATGAC-3',

3'-arm_R: 5'- GACGTCGACACAGCACCAGCTGCAGCAACTACC-3'.

The amplified DNAs were inserted into the *EcoR* I-*Bgl* II and *BamH* I-*Sal* I sites of the HR410PA-1 targeting vector, which carries the GFP expression cassette and puromycin resistance gene between the homology arms. Transfection and selection were performed as described above.

Pull-Down Assays and Immunoblotting

For Rac activation assays, MEFs or cancer cells were stimulated with PDGF (50 ng/ml; Peprotech) or EGF (100 ng/ml; Peprotech) for the specified times. Cells were then lysed by adding 1x MLB ($Mg2^+$ Lysis Buffer: 25 mM Hepes [pH 7.5], 150 mM NaCl, 1% Igepal CA-630, 10 mM $MgCl_2$, 1 mM EDTA, 10% glycerol; Millipore), followed by centrifugation at 20,000 x g for 1 min at 4°C. In some experiments, cells were pretreated with TBOPP (50 μM) or vehicle alone (DMSO; 0.2%). Aliquots were saved for total cell lysate controls, and the remaining lysates were incubated with agarose beads containing the GST-fusion Rac binding domain of PAK1 (#14-325, Millipore) at 4°C for 1 hr. The beads were washed twice with 1x MLB buffer and suspended in SDS-PAGE sample buffer (125 mM Tris-HCl [pH 6.8], 4% SDS, 20% glycerol, 0.01% bromophenol blue, 5% 2-mercaptoethanol). The bound proteins and total cell lysates were separated by SDS-PAGE on a 12.5% polyacrylamide gel, and blots were probed with a monoclonal antibody for Rac1 (23A8, 1:2000 dilution; Millipore).

To examine the effect of TBOPP on association between Rac1 and each Rac GEF, recombinant protein encoding His-SUMO tagged DOCK1 DHR-2, DOCK2 DHR-2, and Tiam1 DH-PH (each 3 μg) was incubated with TBOPP (final 100 μM), compound **5**, or DMSO (2%) in 200 μl of binding buffer (20 mM MES-NaOH, pH 7.0, 150 mM NaCl, 2.5 mM EDTA, 0.0001% Tween-20) for 20 min at room temperature. The samples were then mixed with GST-Rac1-immobilized beads (8 μl) in a total 600 μl of the binding buffer, and incubated at room temperature for 25 min on a rotating wheel. After the beads were washed twice with 600 μl of the binding buffer, bound proteins were separated by SDS-PAGE and blotted with the HisProbe HRP conjugate (1:1000 dilution).

To examine expression and activation of each signaling molecule, cells were lysed on ice in 20 mM Tris-HCl buffer (pH 7.5) containing 1% Triton X-100, 150 mM NaCl, 1 mM EDTA, 1 mM EGTA, 2.5 mM sodium pyrophosphate, 1 mM β-glycerophosphate, 1 mM Na_3VO_4, and complete protease inhibitors (Roche). After centrifugation, the supernatants were mixed with an equal volume of 2x sample buffer (125 mM Tris-HCl, 0.01% bromophenol blue, 4% SDS, 20% glycerol and 200 μM dithiothreitol).

Samples were boiled for 5 min and analyzed by immunoblotting with the following antibodies: rabbit anti-DOCK1 (C4C12; 1:1,000 dilution; Cell Signaling Technology), mouse anti-Tiam1 (E-7; 1:1,000 dilution; Santa Cruz), mouse anti-Ras (RAS10; 1:2,000 dilution; Millipore), rabbit anti-Akt (1:2,000 dilution; Cell Signaling Technology), rabbit anti-phospho-Akt (T308; 1:2,000 dilution; Cell Signaling Technology), rabbit anti-p44/42 MAPK (Erk1/2) (1:2,000 dilution; Cell Signaling Technology), rabbit anti-phospho-p44/42 MAPK (Erk1/2) (T202/Y204; 1:2,000 dilution; Cell Signaling Technology), rabbit anti-p38 MAPK (1:2,000 dilution; Cell Signaling Technology), rabbit anti-phospho-p38 MAPK (T180/Y182; 1:2,000 dilution; Cell Signaling Technology), rabbit anti-SAPK/JNK (1:2,000 dilution; Cell Signaling Technology), mouse anti-phospho-SAPK/JNK (T183/Y185; 1:2,000 dilution; Cell Signaling Technology), and goat anti-β-actin (I-19; 1:2,000 dilution; Santa Cruz) and anti-FLAG (1:2,000 dilution; MBL) antibodies. Polyclonal anti-DOCK5 antibody (1:2,000 dilution) was previously described (Ogawa et al., 2014).

Metabolite Analysis by Ion-Pair Liquid Chromatography Mass Spectrometry

Cells were plated in 6-well plates at a density of 33,000 cells per well. 32 hr after seeding, cells were rinsed briefly with PBS and incubated in the glutamine-deprivation medium. In some experiments, cells were treated with BPTES (10 μM; Sigma-Aldrich). 12-15 hr after medium change, cultured cells were quenched using ice-cold 90% methanol containing 10 mM 2-morpholinoethanesulfonic acid as internal standards (IS) and harvested. The metabolites were analyzed by liquid chromatography mass spectrometry (LC–MS) employing the ion–pair LC mode. The samples were separated on a ACQUITY BEH C18 column (100 mm×2.1 mm I.D., 1.7 μm particle size; Waters) and analyzed using LCMS 8040 instrument (Shimadzu, Japan) in the multiple reaction monitoring (MRM) of 83 specific negative ions including glutamine. The mobile phase was 15 mM acetic acid and 10 mM tributylamine, pH 6.0 (A) and 100% methanol (B). The gradient elution program was as follows: 0–3 min, 0% B; 3–5 min, 0–40% B; 5–7 min, 40–95% B; 7–8 min, 95% B; 8.1–12 min, 0% B. The flow rate was 0.3 ml/min, and the column oven temperature was 40°C. Data processing was carried out using LabSolutions software (Shimadzu).

Chemotaxis Assays

Transwell chemotaxis assays were performed using CCL21 (300 ng/ml) as a chemoattractant, as described previously (Fukui et al., 2001). Briefly, spleen cells (1×10^6) were suspended in serum-free medium and loaded into the upper chamber with 5 μm pore size (Coaster). After incubation for 2 hr at 37°C, spleen cells migrated to the lower chamber were collected and stained for Thy1.2. The percentage

of migrated cells was calculated by dividing the number of Thy1.2$^+$ T cells in the lower chamber by the number of input Thy1.2$^+$ T cells.

Flow Cytometry

The following antibodies were used at the indicated concentrations: phycoerythrin (PE)–conjugated anti-mouse Thy1.2 (CD90.2; 30-H12; 0.4 μg/ml; BD Bioscience) and allophycocyanin (APC)–conjugated CD45R/B220 (RA-3-6B2; 2 μg/ml; TONBO Biosciences). Before staining with the antibodies, cells were incubated for 10 min on ice with anti-Fcγ III/II receptor (2.4G2; 0.5 μg/ml; TONBO Biosciences) to block Fc receptors. Flow cytometric analyses were done on FACS Calibur (BD Bioscience).

Circular Ruffle Formation Assays

MEFs were seeded on fibronectin-coated glass bottom dishes. After serum starvation overnight, cells were stimulated with PDGF (50 ng/ml) for 7 min. Cells were then fixed with 4% paraformaldehyde for 10 min, permeabilized with 0.2% Triton X-100-PBS for 5 min, blocked with 1% bovine serum albumin (BSA)-PBS for 1 hr, and stained with Alexa Fluor 546-conjugated phalloidin (Invitrogen). Samples were analyzed with a laser scanning confocal microscope (LSM510 META).

Supplemental References

Flower, D.R. (1998). On the properties of bit string-based measures of chemical similarity. J. Chem. Inf. Comput. Sci. *38*, 379-386.

Friesner, R.A., Banks, J.L., Murphy, R.B., Halgren, T.A., Klicic, J.J., Mainz, D.T., Repasky, M.P., Knoll, E.H., Shelley, M., Perry, J.K., et al. (2004). Glide: a new approach for rapid, accurate docking and scoring. 1. Method and assessment of docking accuracy. J. Med. Chem. *47*, 1739-1749.

Hawkins, P.C.D., Skillman, A.G., Warren, G.L., Ellingson, B.A., and Stahl, M.T. (2010). Conformer generation with OMEGA: algorithm and validation using high quality structures from the protein databank and Cambridge structural database. J. Chem. Inf. Model. *50*, 572-584.

Lipinski, C.A. (2004). Lead- and drug-like compounds: the rule-of-five revolution. Drug Discov. Today Technol. *1*, 337-341.

Lipinski, C.A., Lombardo, F., Dominy, B.W., and Feeney, P.J. (2001). Experimental and computational approaches to estimate solubility and permeability in drug discovery and development settings. Adv. Drug Deliv. Rev. *46*, 3-26.

Ogawa, K., Tanaka, Y., Uruno, T., Duan, X., Harada, Y., Sanematsu, F., Yamamura, K., Terasawa, M., Nishikimi, A., Côté, J.F., et al. (2014). DOCK5 functions as a key signaling adaptor that FcεRI signals to microtuble dynamics during mast cell degranulation. J. Exp. Med. *211*, 1407-1419.

Rush, T.S., Grant, J.A., Mosyak, L., and Nicholls, A. (2005). A shape-based 3-D scaffold hopping method and its application to a bacterial protein-protein interaction. J. Med. Chem. *48*, 1489-1495.